CrystEngComm

Accepted Manuscript

This article can be cited before page numbers have been issued, to do this please use: K. Chen, Z. Hua, R. Li, Y. Peng, Z. Q. Zhu, J. Zhao and C. Redshaw, *CrystEngComm*, 2020, DOI: 10.1039/D0CE01456G.

ROYAL SOCIETY OF CHEMISTRY

rsc.li/crystengcomm

Assemblies of Cucurbit[6]uril-Based Coordination Complexes with Disulfonate Ligands: From Discrete Complexes to One- and Two-Dimensional Polymers

Kai Chen*, [1], Zi-Yi Hua,[1] Ran Li, [1] Yu-Ying Peng,[1] Qiang Zhao Zhu,[1] Jiang-Lin Zhao*, [2], Carl Redshaw[3]

[1] Collaborative Innovation Center of Atmospheric Environment and Equipment Technology, Jiangsu Key Laboratory of Atmospheric Environment Monitoring and Pollution Control, School of Environmental Science and Engineering, Nanjing University of Information Science & Technology, Nanjing 210044, China.

[2] Institute of Biomedical & Health Engineering, Shenzhen Institutes of Advanced Technology, Chinese Academy of Sciences, 1068 Xueyuan Avenue, Shenzhen 518055, China.

‡ Department of Chemistry & Biochemistry, University of Hull, Hull HU6 7RX, UK.

ABSTRACT: In this work, the combination of cucurbit[6]uril (Q[6]) with varied naphthalene disulfonates and alkaline-earth metal ions allows for successful isolation of 9 novel Q[6]-based coordination complexes with formulas of $[Ca(H_2O)_4(Q[6])_{0.5}(1,5\text{-NDA})_{0.5}]\cdot(1,5\text{-NDA})_{0.5}\cdot 3H_2O$ (**1**), $[Sr(H_2O)_4(Q[6])_{0.5}(1,5\text{-NDA})_{0.5}]\cdot(1,5\text{-NDA})_{0.5}\cdot 4H_2O$ (**2**), $[Ba(H_2O)_4(Q[6])_{0.5}(1,5\text{-NDA})_{0.5}]\cdot(1,5\text{-NDA})_{0.5}\cdot 4H_2O$ (**3**), $[Ca(H_2O)_5(Q[6])_{0.5}](2,6\text{-NDA})\cdot 9H_2O$ (**4**), $[Sr(H_2O)_5(Q[6])_{0.5}]\cdot(2,6\text{-NDA})\cdot 6H_2O$ (**5**), $[Ba_2(H_2O)_7(Q[6])(2,6\text{-NDA})_2]\cdot 11H_2O$ (**6**), $[Sr(H_2O)_4(Q[6])_{0.5}(2,6\text{-NDA})_{0.5}]\cdot(2,6\text{-NDA})_{0.5}\cdot 5H_2O$ (**7**), $[Ca_2(H_2O)_{10}(Q[6])](2,7\text{-NDA})\cdot 14H_2O$ (**8**) and $[Sr(H_2O)_5(Q[6])(2,7\text{-NDA})]\cdot 4H_2O$ (**9**) (H_2NDA = naphthalene disulfonic acid). Structural analysis revealed that the carbonyl groups of Q[6] bind directly to the alkaline-earth metal ions to form 1D coordination chains. Moreover, the metal ions are also linked to the disulfonate substituents of the naphthalenes, which, in the case of **9**, resulted in a simple coordination complex, for **6**, a 1D Q[6]-NDA-M^{2+} chain, and in the case of **1** - **3** and **7**, 2D networks. By contrast, for **4**, **5** and **8**, the disulfonate ligands do not bind

to the metals, and instead, act as supramolecular linkers. The resultant 3D supramolecular architecture of these compounds were constituted through various noncovalent interactions, particularly involving outer-surface interactions of the Q[6]s. Furthermore, the fluorescent properties of the species **2** and **7** were investigated, and sensing experiments indicated that both were capable of functioning as fluorescent sensors for Fe^{3+} with high sensitivity and selectivity.

Keywords: cucurbit[6]uril; coordination complexes; alkaline-earth metal ions; disulfonate ligands; fluorescence sensing.

INTRODUCTION

Cucurbit[*n*]urils (Q[*n*]s) are pumpkin-shaped macrocycles comprising *n* glycoluril units bridged by 2*n* methylene groups and feature a rigid hydrophobic cavity and two polar portals lined with carbonyl groups.[1] Given this extraordinary structure, Q[*n*]s have attracted great interest in the fields of supramolecular and coordination chemistry since the first member Q[6] and other homologues Q[*n*] (n = 5, 7, 8, 10) were successively synthesized, separated and characterized. The majority of the studies on Q[*n*]s are based on the utilization of the hydrophobic cavity and the polar portals.[2-9] In terms of Q[*n*]-based coordination chemistry, numerous Q[*n*]-based coordination complexes have been reported, especially species showing strong affinity for alkali, alkaline-earth and rare earth metal ions.[4, 8-15]

Despite these achievements, there remain many challenges that need to be addressed in the field of Q[*n*]-based coordination chemistry, one of which is the difficulty associated with the construction of high dimensional Q[*n*]-based coordination polymers.[15-17] As far as we know, most of the reported Q[*n*]-based coordination complexes are constructed by the direct coordination of metal ions to Q[*n*]s and form either simple coordination complexes, such as molecular “bowls”, “capsules”, “dumbbells” or one-dimensional chains,[12, 18-23] while two-dimensional (2D) and three-dimensional (3D) coordination polymers are scant.[13, 24-28] The

reason for this is likely the tendency for a convergent arrangement of the carbonyl groups and the resultant opposed coordination orientations.[29] Previous studies have shown that the introduction of a third species can be an effective strategy to overcome this limitation because not only the third species could play a structure-directing role to assist the Q[*n*]s in binding directly to metal ions, but also some of them can utilize their coordination sites and could function as bridging agents to link Q[*n*]-based coordination complexes into high-dimensional coordination polymers.[15, 30-34] For example, Thuéry introduced dicarboxylic acids as the second ligand during the reaction of Q[6] with uranyl ions and successfully obtained a series of 2D Q[6]-based coordination polymers.[30, 35] Using a similar strategy, Fedin also synthesized a series of 1D and 2D Q[6]-based coordination polymers by using terephthalic acid as the auxiliary ligand.[36]

When compared to the use of carboxylate ligands, disulfonate linkers have rarely been investigated, likely due to their weaker coordination strength which has been thought to hinder their ability to act as building blocks in the construction of coordination polymers.[37-40] However, because disulfonate groups have more oxygen atoms that can potentially bind to metal ions and given these oxygen atoms are nonplanar, this means that disulfonate linkers have increased versatility in terms of coordination modes, which in turn allows for the construction of coordination polymers with more diverse architectures.[41-44] Furthermore, sulfonate-based coordination polymers usually show good water-stability over a wide pH and temperature range.[37] Previous studies have also demonstrated that sulfonate ligands are capable to function as supramolecular linker to construct Q[n]-based supramolecular assemblies.[40,44,45] Herein, we have attempted to introduce disulfonate linkers via the use of naphthalene disulfonic acids (H_2NDA), including 1,5-H_2NDA, 2,6-H_2NDA and 2,7-H_2NDA derivatives (**Scheme 1**) into Q[*n*]-M^{2+} (M = Ca, Sr and Ba) type systems. On reaction of H_2NDA with Q[6] and alkaline-earth metal ions, we obtained a series of Q[6]-based coordination complexes in which the

carbonyl groups of Q[6] were directly bound to the metal ions, namely $[Ca(H_2O)_4(Q[6])_{0.5}(1,5\text{-}NDA)_{0.5}]\cdot(1,5\text{-}NDA)_{0.5}\cdot 3H_2O$ (**1**), $[Sr(H_2O)_4(Q[6])_{0.5}(1,5\text{-}NDA)_{0.5}]\cdot(1,5\text{-}NDA)_{0.5}\cdot 4H_2O$ (**2**), $[Ba(H_2O)_4(Q[6])_{0.5}(1,5\text{-}NDA)_{0.5}]\cdot(1,5\text{-}NDA)_{0.5}\cdot 4H_2O$ (**3**), $[Ca(H_2O)_5(Q[6])_{0.5}(2,6\text{-}NDA)]\cdot 9H_2O$ (**4**), $[Sr(H_2O)_5(Q[6])_{0.5}]\cdot(2,6\text{-}NDA)\cdot 6H_2O$ (**5**), $[Ba_2(H_2O)_7(Q[6])(2,6\text{-}NDA)_2]\cdot 11H_2O$ (**6**), $[Sr(H_2O)_4(Q[6])_{0.5}(2,6\text{-}NDA)_{0.5}]\cdot(2,6\text{-}NDA)_{0.5}\cdot 5H_2O$ (**7**), $[Ca_2(H_2O)_{10}(Q[6])(2,7\text{-}NDA)]\cdot 14H_2O$ (**8**) and $[Sr(H_2O)_5(Q[6])(2,7\text{-}NDA)]\cdot 4H_2O$ (**9**) (NDA = naphthalene disulfonic acid). In these complexes, with the exception of **4**, **5**, and **8**, the direct coordination of alkaline-earth metal ions, Q[6] and disulfonate NDA^{2-} ligand generated different coordination structures including a ternary discrete complex (for **9**), a 1D (for **6**) and a 2D (**1-3**, and **7**) coordination polymer. These coordination complexes are then able to form 3D supramolecular architectures via non-covalent interactions. As for complexes **4, 5** and **8**, the Sr^{2+} are only bound to the Q[6] molecules and form 1D Q[6]-Sr^{2+} chains with the disulfonate ligands played the role of a supramolecular linker by forming non-covalent interactions with the outer surface of the Q[6] to afford the final supramolecular architecture. Furthermore, the fluorescence properties of the 2D coordination polymers **2** and **7** have been investigated herein, and both were found to be capable of the detection of Fe^{3+} with high sensitivity and selectivity.

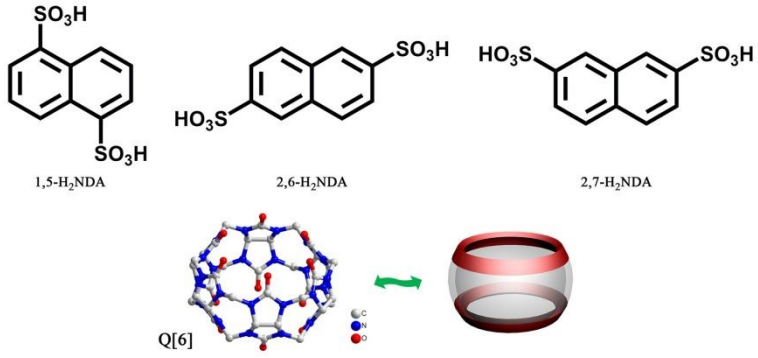

Scheme 1. The naphthalenedisulfonic acid: 1,5-H_2NDA, 2,6-H_2NDA and 2,7-H_2NDA; two representations of the Q[6] molecule.

EXPERIMENTAL SECTION

View Article Online
DOI: 10.1039/D0CE01456G

Materials and methods

All reagents including the sulfonates and solvents were commercially purchased and were used as received without further purification. Q[6]·10H_2O was synthesized according to the previously reported literature method.[46] Elemental analyses for C, H and N were performed on a Perkin-Elmer 240C Elemental Analyzer at the analysis centre of Nanjing University. FT-IR spectra were recorded in the range of 400-4000 cm^{-1} on a Bruker Vector 22 FT-IR spectrophotometer using KBr pellets. Thermogravimetric analyses (TGA) were conducted on a Mettler-Toledo (TGA/DSC1) thermal analyzer under nitrogen with a heating rate of 10 °C·min^{-1}. Powder X-ray diffraction (PXRD) data for all samples were collected at room temperature on bulk samples with Cu Kα radiation (1.54059 Å) on a Bruker D8 Advance X-ray diffractometer, in which the X-ray tube was operated at 40 kV and 40 mA. The fluorescence spectra were recorded on a Perkin Elmer LS-55 fluorescence spectrophotometer. UV-vis measurements were carried out at room temperature on a Shimadzu UV3600 spectrophotometer. Fluorescence lifetime measurements were performed on a HORIBA JobinYvon Fluoromax-4 spectrometer.

X-ray crystallography

The crystallographic data collections for **1**, **2**, **5-9** were carried out on a Bruker Smart Apex II CCD area-detector diffractometer with graphite-monochromated Mo Kα radiation (λ = 0.71073 Å) using ω-scan technique, while **3** and **4** were collected on a Bruker D8 Venture Photon II diffractometer with graphite-monochromated Ga Kα radiation (λ = 1.34139 Å). The diffraction data were integrated by using the *SAINT* program,[47] which was also used for the intensity corrections for the Lorentz and polarization effects. Semi-empirical absorption correction was applied using the *SADABS* program.[48] The structures were solved by direct methods and all the non-hydrogen atoms were refined anisotropically on F^2 by the full-matrix least-squares technique using the SHELXL-2018 crystallographic software package.[49, 50] Most

of the water molecules in the compounds were omitted using the SQUEEZE option of the PLATON program.[51] The squeezed water molecules are 2, 2, 3, 9, 6, 11, 4, 14, and 7 for compounds **1** - **9**, respectively. All non-hydrogen atoms were refined anisotropically and hydrogen atoms were introduced at the calculated positions. The details of the crystal parameters, data collection and refinements for the complexes are summarized in the Table S1, and selected bond lengths and angles with their estimated standard deviations are listed in Table S2.

Preparation of $[Ca(H_2O)_4(Q[6])_{0.5}(1,5\text{-}NDA)_{0.5}]\cdot(1,5\text{-}NDA)_{0.5}\cdot 3H_2O$ (1). A mixture of $Q[6]\cdot 10H_2O$ (30 mg, 0.025 mmol) and $CaCl_2$ (11.0 mg, 0.1 mmol) in deionized water (10 mL) was stirred at room temperature for 1 h and then 1,5-H_2NDA (9.0 mg, 0.025 mmol) was added. The resulting mixture was sealed in a Teflon-lined stainless-steel vessel and then heated at 160 °C for 3 h. After cooling to room temperature, light yellow block crystals of **1** were obtained in 40 % yield based on $Q[6]\cdot 10H_2O$. Anal. calcd for **1** ($C_{28}H_{38}N_{12}O_{19}S_2Ca$): C, 35.36; H, 4.02; N, 17.68 %. Found: C, 35.48; H, 4.21; N, 17.62 %. Selected IR (KBr pellet, cm^{-1}): 3468 (br, m), 1759 (s), 1487 (s), 1425 (m), 1347 (s), 1332 (s), 1307 (s), 1264 (m), 1242 (s), 1089 (s), 967 (s), 857 (s), 706(m), 632 (m).

Preparation of $[Sr(H_2O)_4(Q[6])_{0.5}(1,5\text{-}NDA)_{0.5}]\cdot(1,5\text{-}NDA)_{0.5}\cdot 4H_2O$ (2). Compound **2** was prepared by the same procedure used for preparation of **1** except that $CaCl_2$ was used instead of $SrCl_2\cdot 6H_2O$ (26.6 mg, 0.1 mmol). Yellow block crystals of **2** were obtained in 42 % yield based on $Q[6]\cdot 10H_2O$. Anal. calcd for **2** ($C_{28}H_{40}N_{12}O_{20}S_2Sr$): C, 33.08; H, 3.97; N, 16.54 %. Found: C, 33.01; H, 4.09; N, 16.48 %. Selected IR (KBr pellet, cm^{-1}): 3472 (br, m), 1750 (s), 1495 (s), 1432 (m), 1368 (s), 1322 (s), 1274 (m), 1202 (s), 1181 (s), 972 (s), 861 (s), 712 (m), 654 (m).

Preparation of $[Ba(H_2O)_4(Q[6])_{0.5}(1,5\text{-}NDA)_{0.5}]\cdot(1,5\text{-}NDA)_{0.5}\cdot 4H_2O$ (3). Compound **3** was prepared by the same procedure used for preparation of **1** except that $CaCl_2$ was used instead

View Article Online
DOI: 10.1039/D0CE01456G

of $BaCl_2$ (20.8 mg, 0.1 mmol). Orange block crystals of **3** were obtained in 35 % yield based on Q[6]·10H_2O. Anal. calcd for **3** ($C_{28}H_{40}N_{12}O_{20}S_2Ba$): C, 31.54; H, 3.60; N, 15.76 %. Found: C, 31.52; H, 3.69; N, 15.68 %. Selected IR (KBr pellet, cm^{-1}): 3488 (br, m), 1762 (s), 1557 (s), 1474(s), 1402 (m), 1354 (s), 1307 (s), 1221 (m), 1208 (s), 1155 (s), 967 (s), 855 (s), 701 (m), 638 (m).

Preparation of $[Ca(H_2O)_5(Q[6])_{0.5}(2,6\text{-}NDA)]\cdot 9H_2O$ (4). Compound **4** was prepared by the same procedure used for preparation of **1** except that 1,5-H_2NDA was used instead of 2,6-H_2NDA (9.0 mg, 0.025 mmol). Colorless needle crystals of **4** were obtained in 38 % yield based on Q[6]·10H_2O. Anal. calcd for **4** ($C_{28}H_{52}N_{12}O_{26}S_2Ca$): C, 31.22; H, 4.87; N, 15.60 %. Found: C, 31.29; H, 4.91; N, 15.66 %. Selected IR (KBr pellet, cm^{-1}): 3467 (br, m), 1757 (s), 1568 (s), 1484(s), 1422 (m), 1368 (s), 1321 (s), 1235 (m), 1212 (s), 1168 (s), 988 (s), 844 (s), 718 (m), 652 (m).

Preparation of $[Sr(H_2O)_5(Q[6])_{0.5}]\cdot(2,6\text{-}NDA)\cdot 6H_2O$ (5). A mixture of Q[6]·10H_2O (30 mg, 0.025 mmol) and 2,6-H_2NDA (9.0 mg, 0.025 mmol) in deionized water (10 mL) was stirred at room temperature for 1 h and then $SrCl_2\cdot 6H_2O$ (26.6 mg, 0.1 mmol) was added. The resulting mixture was sealed in a Teflon-lined stainless-steel vessel and then heated at 180 °C for 6 h. After cooling to room temperature, yellow block crystals of **5** were obtained in 30 % yield based on Q[6]·10H_2O. Anal. calcd for **5** ($C_{28}H_{46}N_{12}O_{23}S_2Sr$): C, 31.41; H, 4.33; N, 15.70 %. Found: C, 31.32; H, 4.41; N, 15.62 %. Selected IR (KBr pellet, cm^{-1}): 3481 (br, m), 1758 (s), 1569 (s), 1468(s), 1398 (m), 1345 (s), 1311 (s), 1219 (m), 1198 (s), 1137 (s), 982 (s), 861 (s), 732 (m), 657 (m).

Preparation of $[Ba_2(H_2O)_7(Q[6])(2,6\text{-}NDA)_2]\cdot 11H_2O$ (6). Compound **6** was prepared by the same procedure used for preparation of **3** except that 1,5-H_2NDA was used instead of 2,6-H_2NDA (9.0 mg, 0.025 mmol). Colorless lump crystals of **6** were obtained in 40 % yield based on Q[6]·10H_2O. Anal. calcd for **6** ($C_{56}H_{60}N_{24}O_{30}S_4Ba_2$): C, 31.25; H, 3.93; N, 15.62 %. Found:

C, 31.12; H, 3.99; N, 15.65 %. Selected IR (KBr pellet, cm^{-1}): 3469 (br, m), 1778 (s), 1624 (s), 1481(s), 1415 (m), 1361 (s), 1316 (s), 1226 (m), 1201 (s), 1161 (s), 972 (s), 848 (s), 715 (m), 652 (m).

Preparation of $[Sr(H_2O)_4(Q[6])_{0.5}(2,6\text{-}NDA)_{0.5}]\cdot(2,6\text{-}NDA)_{0.5}\cdot 5H_2O$ (7). Compound **7** was prepared by the same procedure used for preparation of **5** except that $SrCl_2\cdot 6H_2O$ was used instead of $Sr(NO_3)_2\cdot 6H_2O$. After cooling to room temperature, yellow block crystals of **7** were obtained in 30 % yield based on $Q[6]\cdot 10H_2O$. Anal. calcd for **7** ($C_{28}H_{46}N_{12}O_{23}S_2Sr$): C, 31.41; H, 4.33; N, 15.70 %. Found: C, 31.32; H, 4.41; N, 15.62 %. Selected IR (KBr pellet, cm^{-1}): 3477 (br, m), 1765 (s), 1568 (s), 1492(s), 1421 (m), 1362 (s), 1324 (s), 1213 (m), 1199 (s), 1146 (s), 982 (s), 862 (s), 788 (m), 655 (m).

Preparation of $[Ca_2(H_2O)_{10}(Q[6])(2,7\text{-}NDA)]\cdot 14H_2O$ (8). Compound **8** was prepared by the same procedure used for preparation of **1** except that 1,5-H_2NDA was used instead of 2,6-H_2NDA (9.0 mg, 0.025 mmol). Colorless needle crystals of **8** were obtained in 36 % yield based on $Q[6]\cdot 10H_2O$. Anal. calcd for **8** ($C_{56}H_{85}N_{24}O_{48}S_4Ca_2$): C, 32.48; H, 4.13; N, 16.23 %. Found: C, 32.32; H, 4.32; N, 16.16 %. Selected IR (KBr pellet, cm^{-1}): 3509 (br, m), 1801 (s), 1588 (s), 1463(s), 1422 (m), 1368 (s), 1321 (s), 1260 (m), 1214 (s), 1165 (s), 975 (s), 868 (s), 695 (m), 662 (m).

Preparation of $[Sr(H_2O)_5(Q[6])(2,7\text{-}NDA)]\cdot 7H_2O$ (9). Compound **9** was prepared by the same procedure used for preparation of **2** except that 1,5-H_2NDA was used instead of 2,7-H_2NDA (9.0 mg, 0.025 mmol). Colorless needle crystals of **9** were obtained in 30 % yield based on $Q[6]\cdot 10H_2O$. Anal. calcd for **9** ($C_{46}H_{66}N_{24}O_{30}S_2Sr$): C, 34.81; H, 4.19; N, 21.18 %. Found: C, 34.85; H, 4.24; N, 21.22 %. Selected IR (KBr pellet, cm^{-1}): 3472 (br, m), 1781 (s), 1565 (s), 1464(s), 1433 (m), 1388 (s), 1316 (s), 1262 (m), 1245 (s), 1176 (s), 972 (s), 864 (s), 691 (m), 649 (m).

View Article Online
DOI: 10.1039/D0CE01456G

Fluorescence and sensing experiments. The fluorescence properties of **2** and **7**, as well as the free 1,5-H_2NDA and 2,6-H_2NDA compounds, were investigated in the solid state at room temperature. In order to study their sensing capablity for metal ions, fully ground powder samples of **2** and **7** were dispersed in deionized water ultrasonically to prepare the stable suspension (1 mg·mL^{-1}). The suspension was stirred at a constant rate during the fluorescence measurement for homogeneity. Then the fluorescence spectra in 305 - 550 (for **2**) and 285 - 510 (for **7**) upon excitation at 284 and 267 nm respectively were recorded before and after the addition of the solution containing the different metal ions at room temperature. Each experiment was repeated three times to obtain reliable, reproducible data.

RESULTS AND DISCUSSION

Crystal Structures of $[Ca(H_2O)_4(Q[6])_{0.5}(1,5\text{-}NDA)_{0.5}]\cdot(1,5\text{-}NDA)_{0.5}\cdot 3H_2O$ (1), $[Sr(H_2O)_4(Q[6])_{0.5}(1,5\text{-}NDA)_{0.5}]\cdot(1,5\text{-}NDA)_{0.5}\cdot 4H_2O$ (2) and $[Ba(H_2O)_4(Q[6])_{0.5}(1,5\text{-}NDA)_{0.5}]\cdot(1,5\text{-}NDA)_{0.5}\cdot 4H_2O$ (3). Generally, isomorphic crystals of a selected Q[*n*] with the same main family metal cations can be obtained under the same synthetic conditions. As expected, three isomorphic compounds **1** (Ca^{2+}), **2** (Sr^{2+}) and **3** (Ba^{2+}) can obtained from the Q[6]-M^{2+}-1,5-NDA systems. The asymmetric units (**Fig. 1**) of **1**, **2** and **3**, each contains a molecule of $[Ca(H_2O)_4(Q[6])_{0.5}(1,5\text{-}NDA)_{0.5}]\cdot(1,5\text{-}NDA)_{0.5}\cdot 3H_2O$, $[Sr(H_2O)_4(Q[6])_{0.5}(1,5\text{-}NDA)_{0.5}]\cdot(1,5\text{-}NDA)_{0.5}\cdot 4H_2O$ or $[Ba(H_2O)_4(Q[6])_{0.5}(1,5\text{-}NDA)_{0.5}]\cdot(1,5\text{-}NDA)_{0.5}\cdot 4H_2O$, respectively. As shown in **Fig. 1**, each metal ion adopts a distorted square antiprism geometry surrounded by eight oxygen atoms containing three carbonyl oxygen atoms (**1**: O1, O6, O4#1; **2**: O1, O2, O4#1; **3**: O1, O2, O4#1) from two adjacent Q[6] molecules, one disulfonate oxygen atom (O7) from a 1,5-NDA^{2-} and four oxygen atoms (O1W, O2W, O3W, O4W) from coordinated water molecules. Due to the differences in the cationic radii of Ca^{2+} to Ba^{2+}, they exhibited distinct difference in M-O (M = Ca or Sr) bond lengths (**Table S2**), especially those

between the central metal ions and the oxygen atoms from the carbonyl groups of Q[6]. However, the M(II)-O bond lengths and O-M(II)-O bond angles are very consistent with those found in other rare earth metal-Q[*n*]-assemblies.

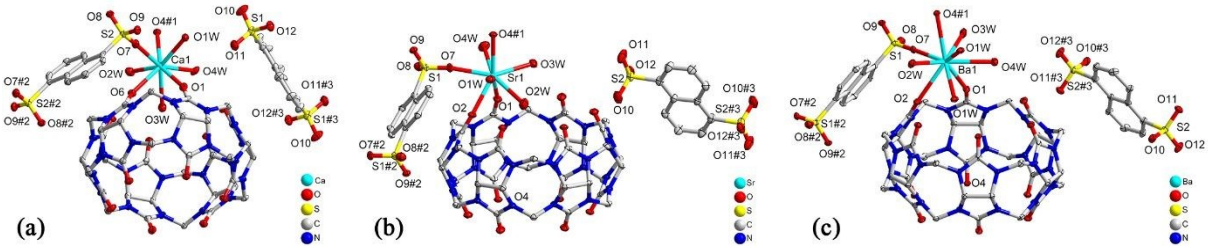

Fig. 1 Coordination environments of M^{2+} in compounds, (a) Ca^{2+} in **1**; (b) Sr^{2+} in **2**; (c) Ba^{2+} in **3**; with the ellipsoids drawn at the 30% probability level. The hydrogen atoms are omitted for clarity. (Symmetry Operators 1#: x+1, y, z; 2#: 2-x, 2-y, 1-z; 3#: 1-x, -y, 2-z for **1**; 1#: x+1, y, z; 2#: 2-x, 2-y, 1-z; 3#: 1-x, -y, 2-z for **2**; 1#: x+1, y, z; 2#: 2-x, 2-y, 1-z; 3#: 1-x, -y, 2-z for **3**.)

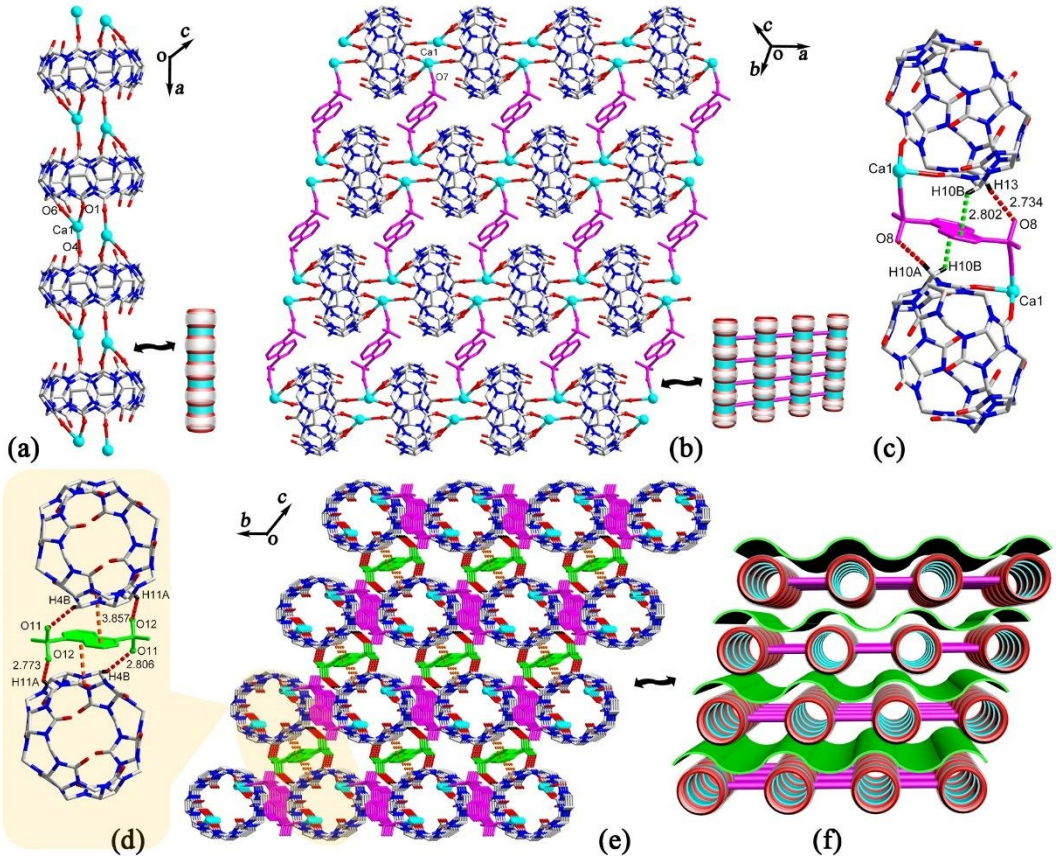

View Article Online
DOI: 10.1039/D0CE01456G

Fig. 2 (a) The 1D Q[6]-Ca^{2+}chain in **1**; (b) The 2D network of **1**; (c) The interactions between the Q[6] and the coordinated 1,5-NDA^{2-}; (d) The interactions between the Q[6] and the free 1,5-NDA^{2-}. (e) The 3D architecture of **1**. (f) Schematic model of **1**. Note: H atoms and water molecules are omitted for clarity.

To further understand the structure of this 2D Q[6]-based supramolecular assembly, the crystal structure of **1** is described in more detail. **Fig. 2a** shows that each carbonyl portal of a Q[6] is linked to two Ca^{2+} cations to generate a one-dimensional Q[6]-Ca^{2+} chain. As for the disulfonate ligand 1,5-NDA^{2-}, it acts as an organic counter anion in the system and has two different chemical environments, namely coordinated (pink) and uncoordinated "free" 1,5-NDA^{2-} (green). As illustrated in **Fig. 2b**, the coordinated 1,5-NDA^{2-} acts as a μ_2-bridging ligand to connect two Ca^{2+} cations from two adjacent chains to form a 2D Q[6]-Ca^{2+}-1,5-NDA^{2-} network. In addition to the electrostatic interactions, there are a plethora of strong non-covalent interactions (C-H···π, 2.802 Å; hydrogen bonding interactions, 2.734 Å; **Fig. 2c**) at the interface between the outer-surface of the Q[6] and 1,5-NDA^{2-} anion, which likely further strengthens the stability of the 2D Q[6]-Ca^{2+}-1,5-NDA^{2-} network. In the case of the free 1,5-NDA^{2-}(**Fig. 2d**: green), they participate in the 2D network through π…π stacking interactions (3.857 Å) between the Q[6] portal carbonyl groups and the naphthalene moieties of 1,5-NDA^{2-} and these are supplemented by hydrogen bonding interactions (2.773 Å) between the disulfonate groups of the free ligand and the methylene groups on the outer surface of the Q[6] (**Fig. 2d**). Hence, the 2D Q[6]-Ca^{2+}-1,5-NDA^{2-} networks can be further linked by the free 1,5-NDA^{2-} to give the final three-dimensional supramolecular architecture of **1** (**Fig. 2e**).

Encouraged by the aforementioned result for the Q[6]-$M_{\text{alkaline earth}}^{2+}$-1,5-$H_2$NDA system, in order to study the effect of changing the organic bridging anion on the nature of the self-assembled network, the use of the related compound 2,6-H_2NDA has been investigated in the Q[6]-$M_{\text{alkaline earth}}^{2+}$ system. As evidenced from the single-crystal structural data of **4** - **7**, only **7**

possessed a 2D structure similar to that observed for **1-3**; the structures of the other systems were very different. These are discussed in more detail below.

Crystal Structures of $[Ca(H_2O)_5(Q[6])_{0.5}(2,6\text{-NDA})]\cdot 9H_2O$ (4) and $[Sr(H_2O)_5(Q[6])_{0.5}]\cdot(2,6\text{-NDA})\cdot 6H_2O$ (5). SC-XRD analysis revealed that **4** and **5** crystallize in the space group $P2_1/n$ with one M^{2+} cation, one half Q[6] molecule, one 2,6-NDA^{2-} ligand and five coordinated water molecules in the asymmetric unit, which are very similar with only the central atom different (**Fig. 3**). Given this, only compound **5** is described here. As shown in **Fig. 3b**, Sr1 is eight-coordinated in a distorted square antiprism geometry formed by three carbonyl atoms (O1, O2, O4#1) from two neighbouring Q[6]s and five coordinated water molecules (O1W, O2W, O3W, O4W, O5W). The coordination between the carbonyl oxygen atoms and Sr^{2+} leads to the formation of one dimension Q[6]-Sr^{2+} chains (**Fig. 4a**). On comparison with compounds **1-3**, it is seen that the disulfonate 2,6-NDA^{2-} anions do not fulfill their "bridging" role by binding to any metal ions but interact with the Q[6] of the Q[6]-Sr^{2+} chains through non-covalent interactions including: (a) the π…π interactions (3.699 Å; **Fig. 4b**) between the carbonyl groups of Q[6] and the naphthalene moieties of 2,6-NDA^{2-}; (b) C-H…π interactions (C11-H11B…π, 3.216 Å; C15-H1…π, 3.493 Å; **Fig. 4b**; C28-H28…π (O8=S1), 3.159 Å; C28-H28…π (O9=S1), 3.249 Å; **Fig. 4c**) between the bridging methylene groups on the outer surface of the Q[6]s and the naphthalene moieties of 2,6-NDA^{2-}; (c) hydrogen bonding interactions (C11-H11B…O10, 2.614 Å; C14-H14B…O10, 2.522 Å; C17-H17B…O7, 2.521 Å; **Fig. 4b**; C5-H5A…O11, 2.222 Å; C6-H6B…O10, 2.996 Å; **Fig. 4c**) between the bridging methylene and methine groups on the outer surface of the Q[6]s and the disulfonate groups of 2,6-NDA^{2-} (**Fig. 4b**). With the assistance of these non-covalent interactions, the final 3D supramolecular framework of **5** is constructed (**Fig. 4e** and **4f**).

View Article Online
DOI: 10.1039/D0CE01456G

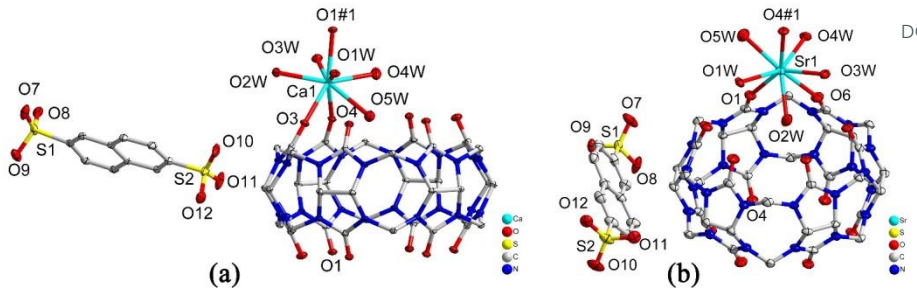

Fig. 3 Coordination environment of M(II) atoms in compounds, (a) Ca^{2+} in **4**; (b) Sr^{2+} in **5**; with the ellipsoids drawn at the 30% probability level. The hydrogen atoms are omitted for clarity. (Symmetry Operators #1: x, 1+y, z)

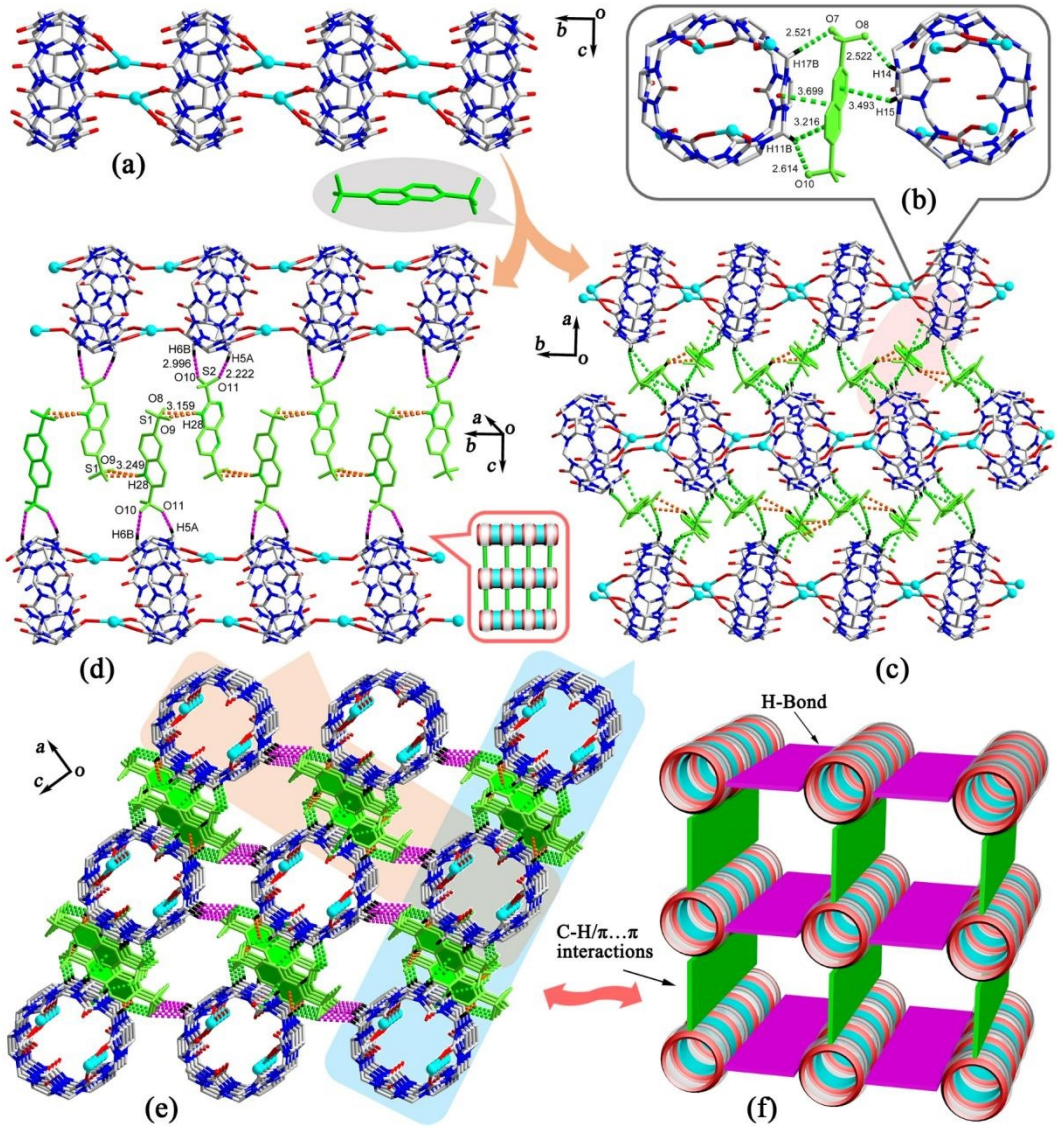

Fig. 4 (a) The 1D Q[6]-Sr^{2+}chain in **5**; (b) Interactions between 2,6-NDA^{2-} and the chains of Q[6]-Sr^{2+}; (c) 2D structure composed of 1D chains of Q[6]-Sr^{2+} connected by H-bond, C-H···π and π-stacking interactions between 2,6-NDA^{2-} and Q[6]; (d) 2D structure showing a "stair" motif composed of 1D chains of Q[6]-Sr^{2+}

View Article Online
DOI: 10.1039/D0CE01456G

connected by H-bond and C-H···π interactions between 2,6-NDA^{2-} and Q[6]; (e) The final 3D supramolecular framework of **5** held by H-bond, C-H···π and π-stacking interactions. (f) Schematic model of **5**.

Crystal Structure of $[Ba_2(H_2O)_7(Q[6])(2,6\text{-}NDA)_2]\cdot 11H_2O$ (6). When Ba^{2+} was used in the reaction under the same experimental conditions as those for **4** and **5** in the Q[6]-$M_{alkaline\ earth}^{2+}$-2,6-H_2NDA system, compound **6** was obtained which possessed a different structure and crystallized in the monoclinic crystal system with the space group of *C*2/*c*. The asymmetric unit of **6** contains two Ba^{2+} cations, one Q[6] molecule, two ligand 2,6-NDA^{2-} and six coordinated water molecules. As **Fig. 5** implies Ba1 possesses a distorted double-capped prismatic geometry surrounded by four carbonyl oxygen atoms (O1, O2, O4#1, O5#1) from two Q[6] molecules, one disulfonate oxygen atom (O13) from 2,6-NDA^{2-} and three coordinated water molecules (O1W, O2W, O7W); while Ba2 adopts a distorted square antiprismatic geometry coordinated by three carbonyl atoms (O7, O8, O10#2) belonging to two adjacent Q[6] molecules, one disulfonate oxygen atom (O19) belonging to 2,6-NDA^{2-} and four coordinated water molecules (O3W, O4W, O5W, O6W). Each portal of a Q[6] coordinates with two Ba^{2+} cations and each Ba^{2+} links two Q[6] molecules, which results in the formation of 1D Q[6]-Ba^{2+} chains. Unlike the former compounds **2** and **5**, only one disulfonate groups of the 2,6-NDA^{2-} in **6** is involved in the coordination with Ba^{2+} and 'hangs' on both sides of the 1D Q[6]-Ba^{2+}-2,6-NDA^{2-} chain acting as two wings of a butterfly ("green" and "pink" ligand, **Fig. 6a**). Adjacent 1D Q[6]-Ba^{2+}-2,6-NDA^{2-} chains are further linked into a 2D supramolecular network *via* H-bonds (C5-H5A···O24, 2.689 Å), C-H…π interactions (C36-H36A…π, 3.635 Å) and π…π interactions (C3=O12…π, 3.639 Å, **Fig. 6d**). Furthermore, the 2D supramolecular layers were found to be stacked on top of each other, stabilized through H-bond interactions (C39-H39···O22, 2.735 Å; C48-H48···O14, 2.463 Å;C55-H55···O18, 2.652 Å; **Fig. 6d**) between the disulfonate groups and the hydrogen atoms on the naphthalene moieties from the adjacent 2,6-NDA^{2-} to form a 3D supramolecular structure.

View Article Online
DOI: 10.1039/D0CE01456G

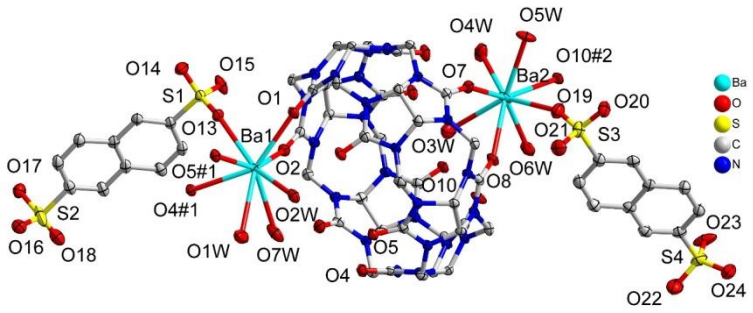

Fig. 5 Coordination environment of Ba(II) atoms in **6** with the ellipsoids drawn at the 30% probability level. The hydrogen atoms are omitted for clarity. (Symmetry Operators 1#: 1-x, y, -z; 2#: 1.5-x+1, 1.5-y, 2-z)

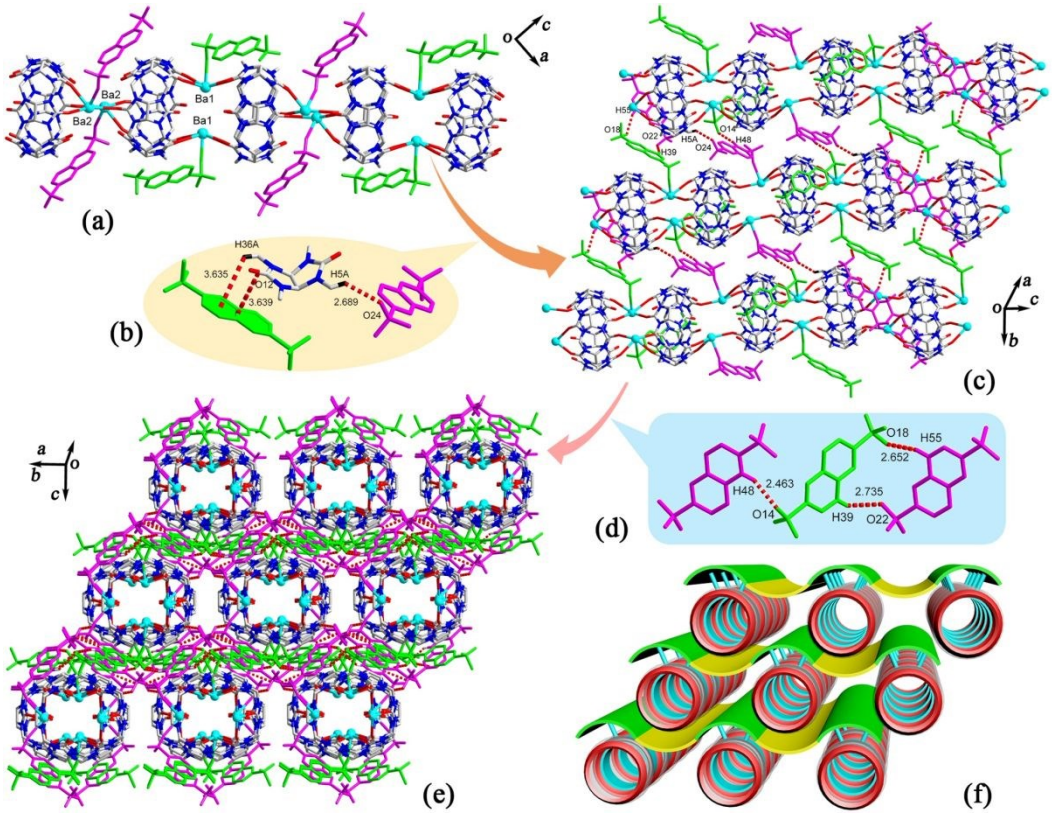

Fig 6. (a) The 1D chain structure of **6**; (b) Interactions between 2,6-NDA^{2-} and Q[6] and the hydrogen bonding between the disulfonate groups and the naphthalene hydrogen atoms of 2,6-NDA^{2-}; (c) 2D structure composed of 1D chains of Q[6]-Ba^{2+} connected by H-bond; (d) The detail interaction between the ligands 2,6-NDA^{2-} and one in neighbouring chain; (e) The 3D supramolecular architecture of **6**; (f) Schematic representation of the 3D framework in **6**.

Crystal Structure of $[Sr(H_2O)_4(Q[6])_{0.5}(2,6\text{-}NDA)_{0.5}]\cdot(2,6\text{-}NDA)_{0.5}\cdot 5H_2O$ (7) Based on our groups previous research results[52, 53], anion control is a promising method for designing and constructing coordination complexes. With the other experimental conditions for synthesizing **5** remaining unchanged, compound **7** which is very similar to compound **5** was obtained by replacing NO_3^- with Cl^-. SC-XRD analysis reveals that **7** crystallizes in the monoclinic crystal system with the space group of $P2_1/n$ and contains a molecule of $[Sr(H_2O)_4(Q[6])_{0.5}(2,6\text{-}NDA)_{0.5}]\cdot(2,6\text{-}NDA)_{0.5}\cdot 5H_2O$ in the asymmetric unit (**Fig. 7**). On comparison with **5**, the only difference is the position of the free anions 2,6-NDA^{2-} in **7**. As shown in **Fig. 8**, the free 2,6-NDA^{2-} (green) connect adjacent 2D networks to afford the final 3D supramolecular architecture (**Fig. 8a**) via non-covalent interactions (**Fig. 8b** and **8c**) between the free disulfonate ligand 2,6-$NDA^{2-}$and the outer-surface of the Q[6]s.

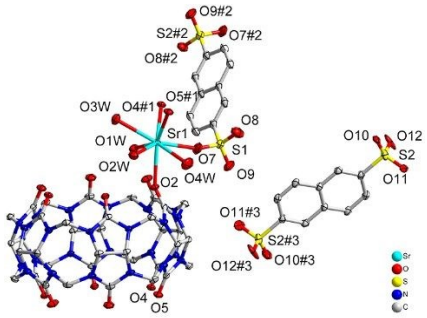

Fig. 7 Coordination environment of Sr^{2+} atoms in **7** with the ellipsoids drawn at the 30% probability level. The hydrogen atoms and free water molecules are omitted for clarity. (Symmetry Operators 1#: x+1, y, z; 2#: 2-x, -y, 1-z; 3#: 1-x, 1-y, 1-z)

View Article Online
DOI: 10.1039/D0CE01456G

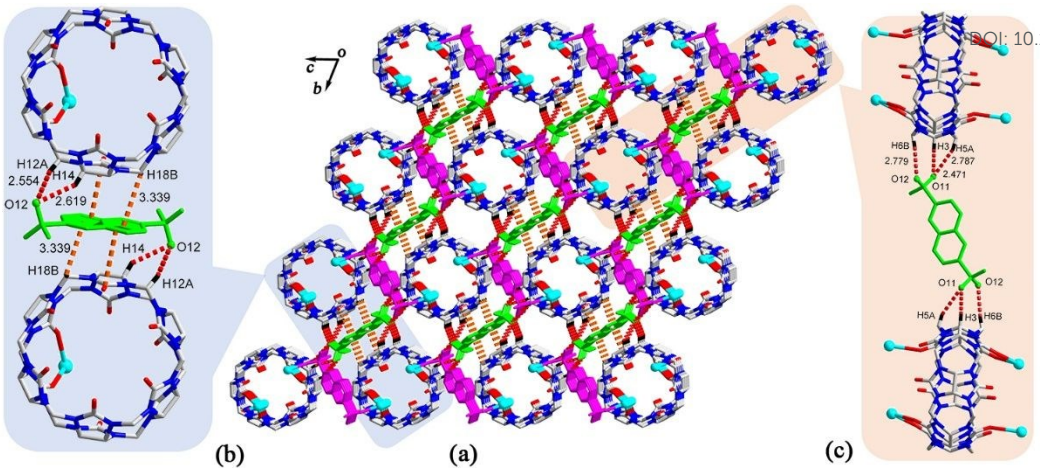

Fig. 8. (a, c) The non-covalent interactions between the free 2,6-NDA2- and neighbouring Q[6]s in **7**; (b) The 3D architecture of **7**.

Crystal Structures of $[Ca_2(H_2O)_{10}(Q[6])(2,7\text{-}NDA)]\cdot 14H_2O$ (8) and $[Sr(H_2O)_5(Q[6])(2,7\text{-}NDA)]\cdot 4H_2O$ (9). We then attempted to form the supramolecular assembly comprised of the Q[6]-$M_{alkaline\ earth}^{2+}$-2,7-H_2NDA system. However, for the Q[6]-$M_{alkaline\ earth}^{2+}$-2,7-H_2NDA system, only Ca(II) and Sr(II)-based supramolecular assemblies' crystals were isolated, which were suitable for X-ray diffraction. X-ray crystallography revealed that **8** crystallizes in the orthorhombic crystal system with the space group of P_{21212} and possesses a different unit cell to **4**; however, their framework structure is similar. The unit cell contains two Ca^{2+} cations, one Q[6] molecule, two free ligands 2,7-NDA^{2-} and ten coordinated water molecules (**Fig. 9**). The crystal packing motif in **8** is somewhat modified by replacing 2,7-NDA^{2-} by 2,6-NDA^{2-}, however, the packing is similar to that of **4** and **5** in which non-covalent interactions between the naphthalene moieties of 2,6-NDA^{2-} and the outer surface of the Q[6] and the carbonyl groups of Q[6] allow the 1D Q[6]-Ca^{2+} chains to form 2D layers and then the final 3D framework (**Fig. 10**). It is evident that the nitrate (NO_3^-) plays an important role in the syntheses of compounds **4** and **7** and its presence may promote the expected structures as **1-3** in which the disulfonate ligands play a bridging role by coordination of disulfonate with the metal ion from adjacent Q[6]-M^{2+} chain.

View Article Online
DOI: 10.1039/D0CE01456G

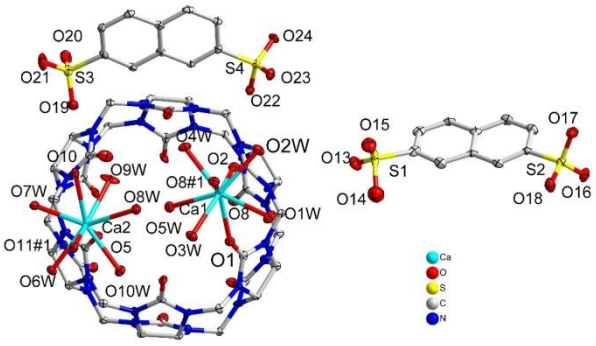

Fig. 9 Coordination environment of Ca^{2+} atoms in **8** with the ellipsoids drawn at the 30% probability level. The hydrogen atoms and free water molecules are omitted for clarity. (Symmetry Operators 1#: x, y, -1+z)

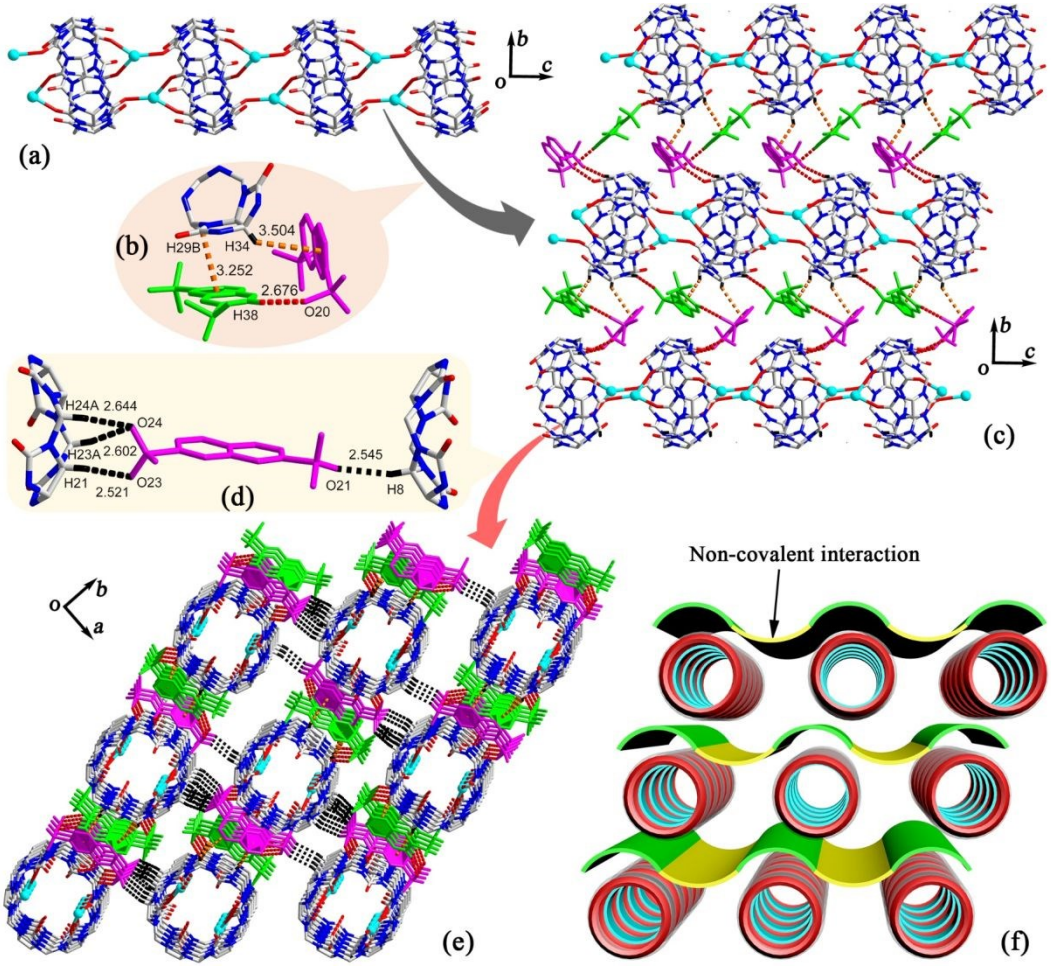

Fig. 10 (a) The 1D chain structure of **8**; (b) Interactions between 2,6-NDA^{2-} and Q[6] and the hydrogen bonding between the disulfonate groups and the naphthalene hydrogen atoms of 2,7-NDA^{2-}; (c) 2D structure composed of 1D chains of Q[6]-Ca^{2+}; (d) The detail interaction between the ligands 2,6-NDA^{2-} and two Q[6]

View Article Online
DOI: 10.1039/D0CE01456G

from neighbouring chain. (e) The 3D supramolecular architecture of **8**. (f) Schematic representation of the 3D framework in **8**.

Compound **9** crystallized in the monoclinic space group $P2_1/n$ and consists of one Sr^{2+} cations, one Q[6] molecule, one ligand 2,7-NDA^{2-} and five coordinated water molecules in the asymmetric unit, and is different from the above compounds **1** - **8**. In **9**, Sr1 is coordinated by two carbonyl oxygen atoms (O1, O2) from the same Q[6] molecule, one disulfonate oxygen atom (O13) from 2,7-NDA^{2-} and five coordinated water molecules (O1W, O2W, O3W, O4W, O5W) in a distorted square antiprism geometry. In the structure, each Sr^{2+} coordinates with only one side carbonyl oxygen of Q[6] and one ligand 2,7-NDA^{2-}, while each Q[6] and 2,7-NDA^{2-} bind to only one Sr^{2+} as well, which results in the formation of a 1:1:1 ternary coordination compound (**Fig. 11**). On further inspection of the structure, the compound comprises 1D supramolecular chains formed via the C12-H12A···π interactions (3.192 Å) between the carbonyl groups of Q[6] (**Fig. 12a**) and these chains then interact with each other to give a 2D supramolecular layer through hydrogen bonding (C22-H22···O18, 2.571 Å; C23-H23B···O17, 2.476 Å; C24-H24B···O17, 2.594 Å; C27-H27···O8, 2.850 Å; **Fig. 12b**) between the disulfonate groups and the methylene and methine groups on the outer surface of Q[6]. As the same time, non-covalent interactions originating from strong C-H···π interactions (C14-H14···π, 2.699 Å; C16-H16···π, 2.637 Å; **Fig. 12e** left) and hydrogen bonding interactions (C9-H9···O15, 2.667 Å; C12-H12B···O17, 2.713 Å; C18-H18B···O18, 2.666 Å; **Fig. 12e** left) between the carbonyl groups of Q[6] and the naphthalene moieties of 2,7-NDA^{2-}, as well as strong hydrogen bonding interactions (C2-H2···O9, 2.187 Å; C3-H3···O10, 2.560 Å; C5-H5A···O12, 2.333 Å; C6-H6A···O11, 2.340 Å; C35-H35A···O9, 2.486 Å; **Fig. 12e** right) between two adjacent Q[6], further linked neighbouring layers into the final 3D supramolecular architecture (**Fig. 12f** and **g**).

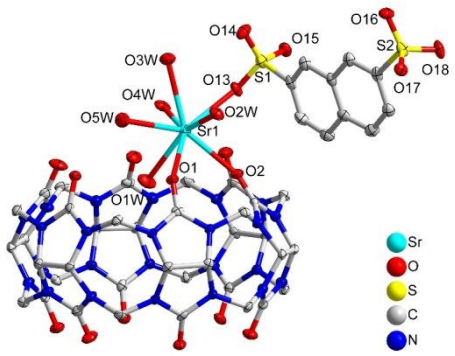

Fig. 11. Coordination environment of Sr(II) atoms in **9** with the ellipsoids drawn at the 30% probability level. The hydrogen atoms are omitted for clarity. (Symmetry Operators A: -x+0.5, -y+0.5, -z; B: -x+1, y, -z +0.5)

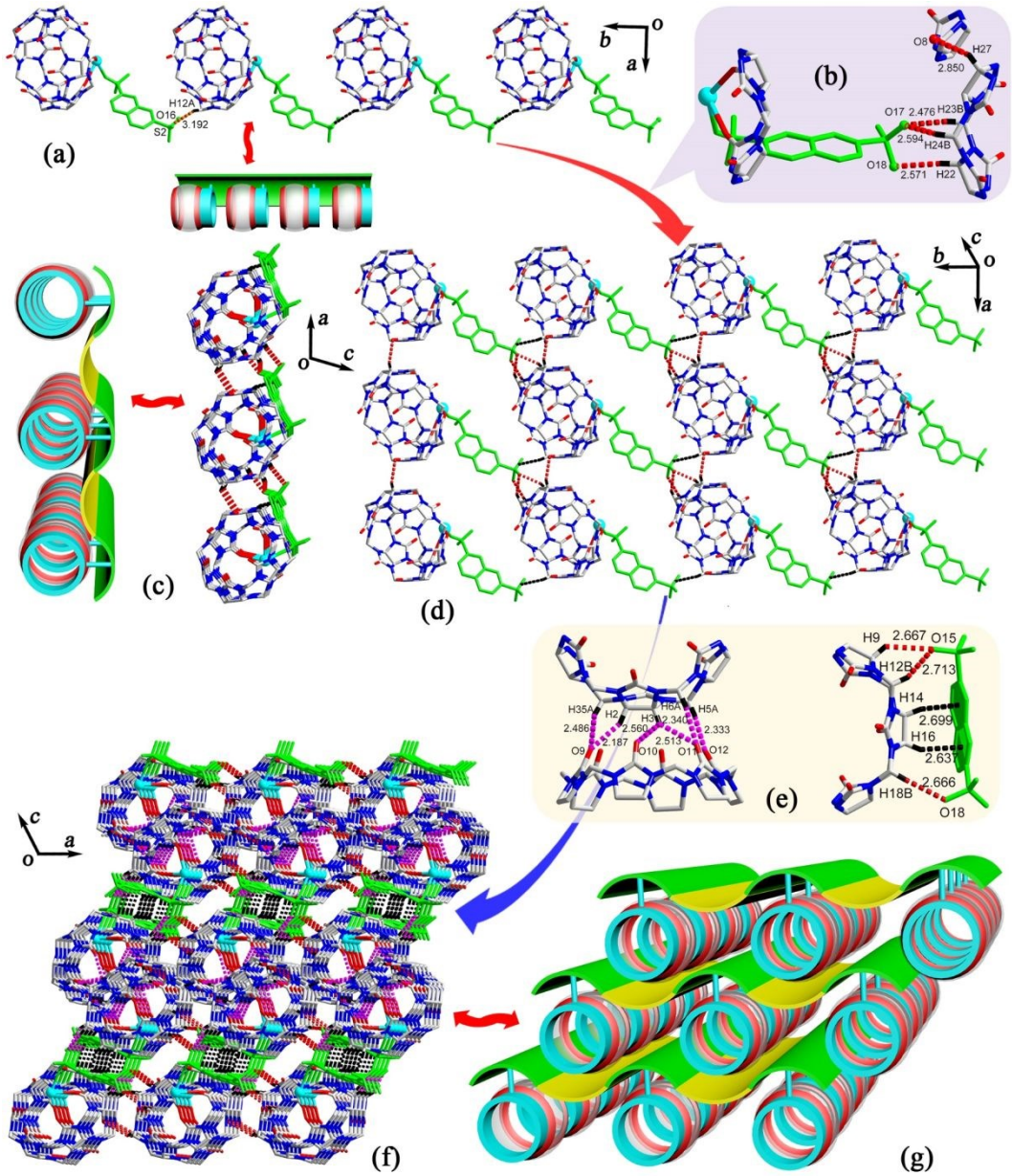

Fig. 12 (a) The 1D chains of **9** constructed from the simple coordination complex through the C-H···π interactions between Q[6]s; (b) The hydrogen bonding between the neighboring 1:1:1 ternary unit; (c) and (d) The 2D supramolecular layer from different direction; (e) The noncovalent between the Q[6] and the 2,7-NDA^{2-} and H-bond between the neighboring Q[6]; (f) The 3D architecture of **9**; (g) Schematic representation of the 3D framework in **9**.

Discussion of the Synthetic Effect

View Article Online
DOI: 10.1039/D0CE01456G

Compounds **1** - **9** were synthesized using the same molar ratio of Q[6], ligand and metal ion via the hydrothermal method. According to the above structural descriptions, it is clear that the ligands 1,5-NDA^{2-}, 2,6-NDA^{2-}, 2,7-NDA^{2-} in the respective compounds act as a counter anion and no inorganic anions are present in the structures (**Scheme 2**). What's more, the alkaline earth metal ions directly coordinate with carbonyl oxygens of Q[6] to form 1D chains in compounds **1**-**8**, which can be linked by coordination between disulfonate and metal ion (**1**-**3** and **7**), or non-covalent interactions between the ligand and Q[6] (**4**-**6** and **8**), or in the case of the Sr(II) compound **9**, coordinated with only one port of a Q[6] to form a simple ternary unit. It should be noted that the non-covalent interactions between the ligand and Q[6] can further construct two adjacent 2D network to afford the final 3D framework, and as such play a pivotal role in controlling the self-assembly process. In addition, for the Q[6]-$M_{alkaline\ earth}^{2+}$-2,6-H_2NDA system, an identical procedure to **7** was followed to the preparation of **5**, except that $SrCl_2$ was changed to $Sr(NO_3)_2$, and surprisingly, compound **7** exhibited the structure as seen for **1**-**3**. Taking this together, it can be concluded that the existence of the non-covalent interactions in these supramolecular self-assemblies are pivotal to their formation.

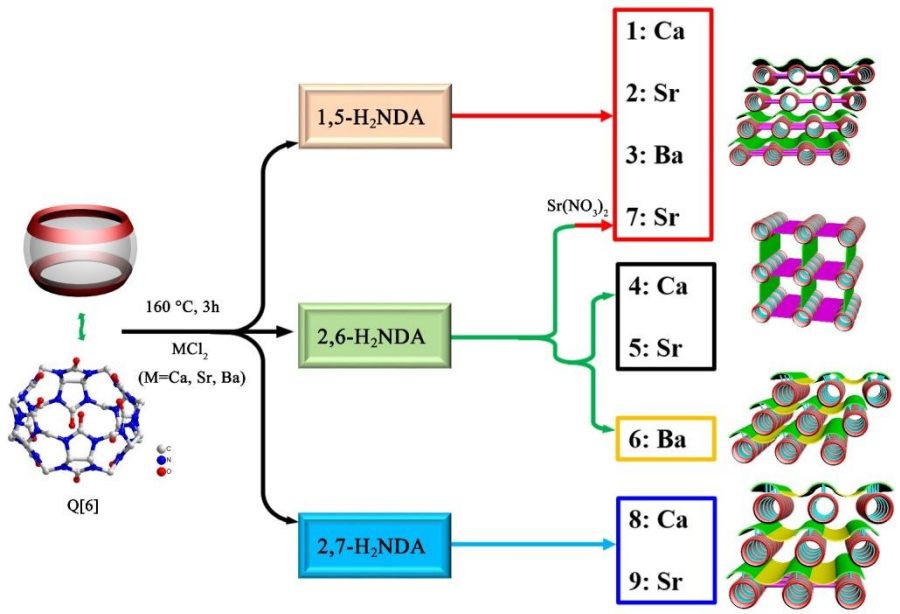

Scheme 2. the synthesis methods of nine complexes and their structures classification.

View Article Online
DOI: 10.1039/D0CE01456G

Powder X-ray diffraction (PXRD) and stability studies. PXRD measurements were employed to confirm the bulk-phase purity of the as synthesized **1-9**. As showed in **Fig. S1**, the results of PXRD measurements revealed that the peak positions of the obtained crystalline samples of **1-9** closely matched the simulated data, confirming the phase purity of the synthesized samples.

The thermal stability of **1-9** was examined by thermogravimetric analysis (TGA) and the results are given in **Fig. S2**. For compounds **1-3**, the first obvious weight loss below 200 °C can be attributed to the free and coordinated water loss (**1**: obsd:13.14 %, calcd: 13.25%; **2**: obsd:14.09%, calcd: 14.16%; **3**: obsd:13.43%, calcd: 13.51%), which are in accordance with the results of the SC-XRD analysis, and each system is stable up to about 445, 438 and 431 °C, respectively. While for compounds **4 - 7**, the TG curves display a weight loss of 23.12 % (**4**), 18.32 % (**5**), 15.04 % (**6**), 15.06 % (**7**) from 30 to 240 °C, suggesting the release of the coordinated water molecules (calcd 23.39%; 18.38%, 15.05%; 15.13%) and their frameworks begin decomposing at about 420 °C, except for **7** at 430 °C. Compounds **8** and **9** show similar thermal degradation curves, with the first weight loss of 20.41% (calcd: 20.86%) for **8** and 9.86 % (calcd: 10.21%) for **9** that can be ascribed to the removal of free and coordinated water molecules, and then the frameworks are stable up to about 420 °C and 426 °C, respectively.

Fluorescence sensing capacity of 2 and 7. As illustrated in the structural analysis, all the compounds **1-3** and **7** are constructed from 2D Q[6]-NDA-M^{2+} coordination networks and the metal ions used in compounds **2** and **7** are the same. Therefore, the solid-state fluorescence properties of **2** and **7** were examined at room temperature. The fluorescence emission maxima of 1,5-H_2NDA and 2,6-H_2NDA were observed at 401 and 387 nm upon excitation at 368 and 347 nm, respectively, while complexes **2** and **7** exhibit characteristic emission bands with the maxima at 335 (for **2**) and 314 (for **7**) upon excitation at 296 and 287 nm respectively (**Fig. S3**). The emissions observed in **2** and **7** can be tentatively assigned to the introduced disulfonate

View Article Online
DOI: 10.1039/D0CE01456G

ligands due to their similarity. In addition, compared to the free 'ligands', **2** and **7** exhibit blue-shifted emissions, which can be explained by the fact that intermolecular hydrogen bond[54, 55] would reduce the energy level of every electronic state, leading to the weakening of intermolecular hydrogen bonds in excited states between 1,5-NDA^{2-} or 2,6-NDA^{2-} and Q[6]. This can be explained by the fact that intermolecular hydrogen bonds will reduce the energy level of each electronic state,

Given the existence of "free" disulfonate ligands in the structure and the good fluorescence performance, the sensing capability of complexes **2** and **7** for metal ions was investigated in aqueous system. Prior to the sensing experiments, the as-synthesized samples of **2** and **7** were fully ground and soaked in deionized water with ultrasonic treatment to obtain stable suspensions (1 mg mL^{-1}). The changes of the fluorescence intensity of the suspension (2.5 mL) of **2** and **7** were recorded upon the addition of the solution of different metal ions (1 M, 50 μL), including Na^{+}, K^{+}, Rb^{+}, Cs^{+}, Mg^{2+}, Ca^{2+}, Sr^{2+}, Ba^{2+}, Cr^{3+}, Mn^{2+}, Fe^{2+}, Fe^{3+}, Co^{2+}, Ni^{2+}, Cu^{2+}, Zn^{2+}, Cd^{2+}, Al^{3+} and Pb^{2+} and the changes in the fluorescence emission intensity were calculated by using the formula, $I/I_0 \times 100$ %, where I_0 and I are the maximum fluorescence intensity of **2** and **7** before and after the addition. As depicted in **Fig. 13**, the fluorescence performance of **2** and **7** exhibited significantly different response to these selected metal ions. In the presence of alkali and alkaline-earth metal ions, little enhancement in the intensity of the fluorescence emissions of **2** and **7** was observed, while the intensities of emissions of **2** and **7** in the presence of other metal ions except Fe^{3+} showed slight or moderate reduction. As for Fe^{3+}, it can be observed that it could almost completely quench the fluorescence emission of **2** and **7**.

View Article Online
DOI: 10.1039/D0CE01456G

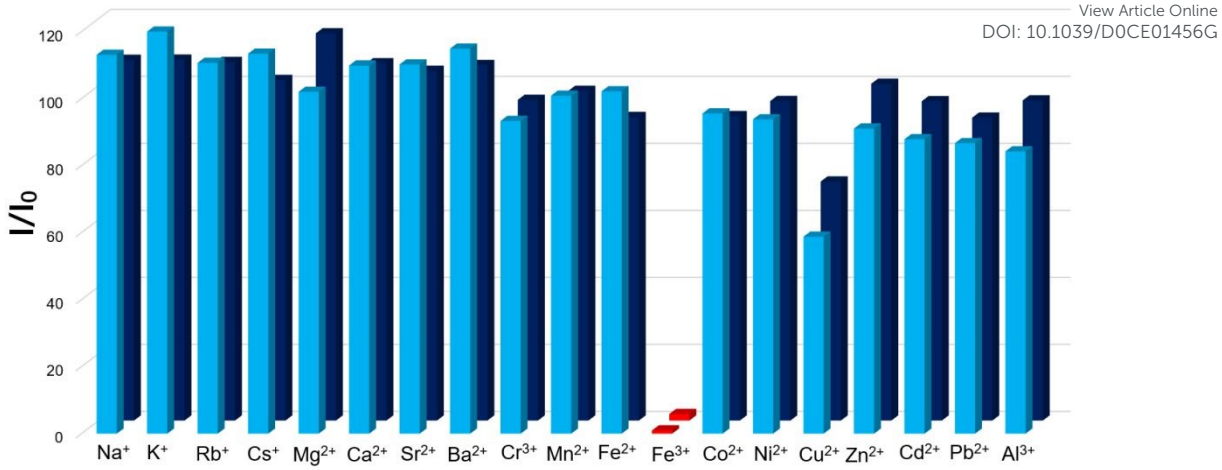

Fig. 13 The variation of the fluorescence emission intensity of the suspension of **2** and **7** upon addition of different metal ions (inside: complex **7**; outside: complex **2**).

This phenomenon indicated that both the complexes **2** and **7** could detect Fe^{3+} in aqueous systems through fluorescence quenching. In order to assess the sensitivity of **2** and **7** towards Fe^{3+}, quantitative fluorescence titration experiments upon the gradual addition of aqueous solution of Fe^{3+} to the suspension of **2** and **7** were conducted. As **Fig. 14** illustrates, the fluorescence intensities decreased gradually upon the incremental addition of Fe^{3+}. The changes in the relative emission intensities (I_0/I) of **2** and **7** on increasing the concentration of Fe^{3+} in the suspension was plotted, on basis of which the fluorescence quenching constants could be analysed. As shown in **Fig. 15**, the plots of relative intensities *versus* the concentration of Fe^{3+} bent distinctly upward rather than being linear, indicating that the quenching occurred *via* a static pathway or a combination of static and dynamic pathways. Accordingly, the pathway could be easily determined by the lifetime measurement because the fluorescence lifetime would decrease in the case of dynamic quenching but remain unchanged for static quenching.[56] From **Fig. S4**, it can be observed that both of the lifetime of **2** and **7** remained almost the same after the addition of Fe^{3+}, demonstrating the static quenching pathway. Therefore, the nonlinear Stern-Volmer equation, $I_0/I=Ae^{k[Q]} + B$, where A, B and k are constants, was applied to analyzing the quenching constants in this case and the results revealed that the calculation of

View Article Online
DOI: 10.1039/D0CE01456G

experimental data and fitting-curves matched well with the correlation coefficient (R^2) value larger than 0.999. The quenching constants were calculated to be 4.32×10^3 and 4.16×10^3 M^{-1} for **2** and **7**, respectively according to the formula $K_{SV} = A \times k$, which is comparable or even higher than many reported fluorescent sensors [56-66] (**Table S2**). The detection limit (DL) was estimated to be 1.40×10^{-5} M for **2** and 1.96×10^{-5} M for **7** according to the equation, DL=3σ/m, where σ is the standard deviation and m is the slope (**Table S3**).

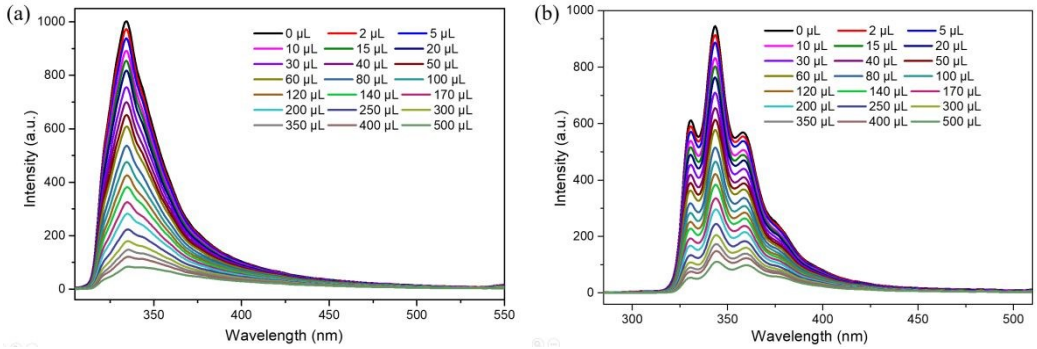

Fig. 14 Changes in emission intensities of **2** (a) and **7** (b) with gradual addition of Fe^{3+}.

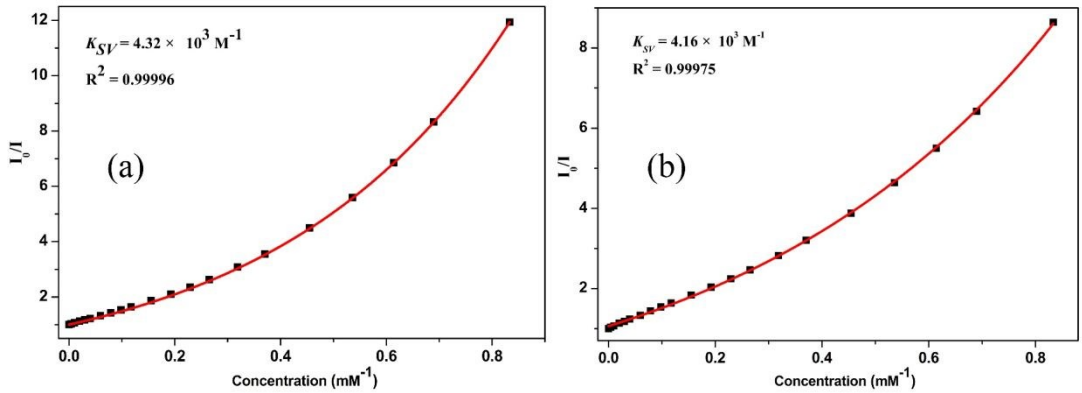

Fig. 15 The relative intensities of **2** (a) and **7** (b) with gradual addition of Fe^{3+}.

In addition, consideration of the recyclability is an important factor for practical applications, the repeatability of **2** and **7** for the detection of Fe^{3+} was also examined. The stability of complexes **2** and **7** in the aqueous solution of Fe^{3+} made it possible for them to be reused (**Fig. S5**). After the sensing experiments, the suspensions of **2** and **7** with Fe^{3+} were centrifuged and washed five times with deionized water. After drying at 80 ℃, the recovered samples of **2** and **7** were used to prepare aqueous suspensions and then reused to detect Fe^{3+}. After five cycles,

View Article Online
DOI: 10.1039/D0CE01456G

no significant loss in the fluorescence intensity was observed and the quenching ability was unaffected, demonstrating the reproducibility of **2** and **7** for the detection of Fe^{3+} (**Fig. S6**).

The mechanism for the quenching effect of Fe^{3+} towards **2** and **7** was then investigated. As mentioned above, the structures of the complexes **2** and **7** are maintained after the addition of Fe^{3+}, hence the collapse of crystalline structures was not the cause of the fluorescence quenching. Secondly, the quick response time indicates that the fluorescence quenching should not be ascribed to metal ion exchange. Furthermore, FT-IR measurements were also carried out to check whether there was coordination between Fe^{3+} and the uncoordinated carbonyl or disulfonate groups in **2** and **7**. As shown in **Fig. S7a**, all the adsorption peaks of **2** and **7** almost remained the same after the addition of Fe^{3+}, which indicated that the Fe^{3+} had not coordinated with the disulfonate groups. Meanwhile, the consistent fluorescence lifetimes of **2** and **7** before and after the addition of Fe^{3+} also confirmed that there was no coordination between the Fe^{3+} and the carbonyl or disulfonate groups of **2** and **7**. In addition, the UV-Vis absorption spectrum of Fe^{3+} ions in aqueous solution have a strong UV-Vis adsorption ability in the 200–450 nm range (**Fig. S7b**). As all the excitation and emission wavelengths of **2** and **7** were in the range 250-400 nm, competition of absorption and resonance energy transfer is possible and can lead to fluorescence quenching. A similar mechanism for the luminescent quenching has also been found in our previous research and in other reported compounds.[55, 56, 66, 67]

CONCLUSIONS

In this work, we employed the naphthalene disulfonic acids (H_2NDA), namely 1,5-H_2NDA, 2,6-H_2NDA and 2,7-H_2NDA in combination with Q[*n*]-M^{2+} (M = Ca, Sr and Ba) systems and successfully synthesized and structurally characterized nine new Q[6]-based coordination complexes, in which the carbonyl groups of Q[6] were all bound to the alkaline-earth metal ions directly to generate either 1D Q[6]-M^{2+} supramolecular chains (**1-8**) or a simple 1:1 complex Q[6]-Sr^{2+} (**9**). With the exception of **4**, the disulfonate groups of the introduced ligands

View Article Online
DOI: 10.1039/D0CE01456G

also participated in coordination to M^{2+} and Q[6], which allowed for the generation of different coordination structures from ternary discrete complex (for **6**) to 1D (for **5**) and 2D (**1-3**) coordination polymers and these coordination complexes then, via secondary interactions, were able to form the final supramolecular architectures. In complex **4**, the disulfonate ligands functioned as a supramolecular linker to afford the final supramolecular architecture. Furthermore, the fluorescence properties of the 2D coordination polymers **2** and **7** were investigated and the sensing experiments suggested that both can detect Fe^{3+} with high sensitivity and selectivity.

ASSOCIATED CONTENT

Supporting Information

The Supporting Information is available free of charge on the RSC Publication website at DOI: 10.1021/rsc.

PXRD patterns, TG, and additional figures (PDF)

X-ray crystallographic data in CIF format (CIF)

Accession Codes

CCDC: 1986739-1986747 contain the supplementary crystallographic data for this paper. These data can be obtained free of charge *via* www.ccdc.cam.ac.uk/data_request/cif, or by emailing data_request@ccdc.cam.ac.uk, or by contacting The Cambridge Crystallographic Data Centre, 12 Union Road, Cambridge CB2 1EZ, UK; fax: +44 1223 336033.

AUTHOR INFORMATION

Corresponding Author

*E-mail: kaichen85@nuist.edu.cn (K. Chen); jl.zhao@siat.ac.cn (J.-L. Zhao).

ORCID

Kai Chen: 0000-0002-5852-3264; Jiang-Lin Zhao: 0000-0002-9598-051X.

Notes

The authors declare no competing financial interest.

View Article Online
DOI: 10.1039/D0CE01456G

ACKNOWLEDGMENTS

We thank the National Natural Science Foundation of China Grant No. 21601090 and the Natural Science Foundation of Jiangsu Province (BK20160943), Miss Zi-Yi Hua thanks Jiangsu Province Graduate Training Practice Innovation Program (KYCX20_0961), and Miss Yu-Ying Peng thanks the Innovation and Entrepreneurship Training Program of Nanjing University of Information Science and Technology for financial support. Dr. Jiang-Lin Zhao thanks the Basic Research Program of Shenzhen (JCYJ20190812151405298). CR thanks the EPSRC for an overseas travel grant.

REFERENCES

1 J. Lagona, P. Mukhopadhyay, S. Chakrabarti and L. Isaacs, The cucurbit[n]uril family, *Angew. Chem., Int. Ed.*, 2005, **44**, 4844-4870.

2 E. Masson, X. Ling, R. Joseph, L. Kyeremeh-Mensah and X. Lu, Cucurbituril chemistry: a tale of supramolecular success, *RSC Adv.*, 2012, **2**, 1213-1247.

3 S. J. Barrow, S. Kasera, M. J. Rowland, J. del Barrio and O. A. Scherman, Cucurbituril-Based Molecular Recognition, *Chem. Rev.*, 2015, **115**, 12320-12406.

4 W. A. Freeman, W. L. Mock and N. Y. Shih, Cucurbituril, *J. Am. Chem. Soc.*, 1981, **103**, 7367-7368.

5 J. Kim, I. S. Jung, S. Y. Kim, E. Lee, J. K. Kang, S. Sakamoto, K. Yamaguchi and K. Kim, New Cucurbituril Homologues: Syntheses, Isolation, Characterization, and X-ray Crystal Structures of Cucurbit[n]uril (n = 5, 7, and 8), *J. Am. Chem. Soc.*, 2000, **122**, 540-541.

6 A. I. Day and A. P. Arnold, Method for synthesis of cucurbiturils, WO 0068232, 2000, **8**.

7 A. I. Day, R. J. Blanch, A. P. Arnold, S. Lorenzo, G. R. Lewis and I. Dance, A Cucurbituril-Based Gyroscane: A New Supramolecular Form, *Angew. Chem., Int. Ed.*,

View Article Online
DOI: 10.1039/D0CE01456G

2002, **41**, 275-277.

8 X. L. Ni, X. Xiao, H. Cong, L. L. Liang, K. Cheng, X. J. Cheng, N. N. Ji, Q. J. Zhu, S. F. Xue and Z. Tao, Cucurbit[n]uril-based coordination chemistry: from simple coordination complexes to novel poly-dimensional coordination polymers, *Chem. Soc. Rev.*, 2013, **42**, 9480-9508.

9 X. L. Ni, S. F. Xue, Z. Tao, Q. J. Zhu, L. F. Lindoy and G. Wei, Advances in the lanthanide metallosupramolecular chemistry of the cucurbit[n]urils, *Coord. Chem. Rev.*, 2015, **287**, 89-113.

10 Y. Q. Yao, K. Chen, Z. Y. Hua, Q. J. Zhu, S. F. Xue and Z. Tao, Cucurbit[n]uril-based host–guest-metal ion chemistry: an emerging branch in cucurbit[n]uril chemistry, *J. Incl. Phenom. Macrocycl. Chem.*, 2017, **89**, 1-14.

11 X. L. Ni, X. Xiao, H. Cong, Q. J. Zhu, S. F. Xue and Z. Tao, Self-assemblies based on the "outer-surface interactions" of cucurbit[n]urils: new opportunities for supramolecular architectures and materials, *Acc. Chem. Res.*, 2014, **47**, 1386-1395.

12 J. Heo, S. Y. Kim, D. Whang and K. Kim, Shape-Induced, Hexagonal, Open Frameworks: Rubidium Ion Complexed Cucurbituril, *Angew. Chem., Int. Ed.*, 1999, **38**, 641-643.

13 P. Thuéry, Uranyl Ion Complexes with Cucurbit[n]urils (n = 6, 7, and 8): A New Family of Uranyl-Organic Frameworks, *Cryst. Growth Des.*, 2008, **8**, 4132–4143.

14 P. Thuéry, Lanthanide Complexes with Cucurbit[n]urils (n = 5, 6, 7) and Perrhenate Ligands: New Examples of Encapsulation of Perrhenate Anions, *Inorg. Chem.*, 2009, **48**, 4497-4513.

15 K. Chen, L. L. Liang, Y. Q. Zhang, Q. J. Zhu, S. F. Xue and Z. Tao, Novel supramolecular assemblies based on coordination of samarium cation to cucurbit[5]uril, *Inorg. Chem.*, 2011, **50**, 7754-7760.

16 P. Thuéry, Uranyl-Alkali Metal Ion Heterometallic Complexes with Cucurbit[6]uril and a

Sulfonated Catechol, *Cryst. Growth Des.*, 2011, **11**, 3282-3294.

17 K. Chen, Y. F. Hu, X. Xiao, S. F. Xue, Z. Tao, Y. Q. Zhang, Q. J. Zhu and J. X. Liu, Homochiral 1D-helical coordination polymers from achiral cucurbit[5]uril: hydroquinone-induced spontaneous resolution, *RSC Adv.*, 2012, **2**, 3217–3220.

18 D. Whang, J. Heo, J. H. Park and K. Kim, A Molecular Bowl with Metal Ion as Bottom: Reversible Inclusion of Organic Molecules in Cesium Ion Complexed Cucurbituril, *Angew. Chem., Int. Ed.*, 1998, **37**, 78-80.

19 J. X. Liu, L. S. Long, R. B. Huang, L. S. Zheng, Molecular Capsules Based on Cucurbit[5]uril Encapsulating "Naked" Anion Chlorine, *Cryst. Growth Des.*, 2006, **6**, 2611-2614.

20 J. X. Liu, L. S. Long, R. B. Huang and L. S. Zheng, Interesting Anion-Inclusion Behavior of Cucurbit[5]uril and Its Lanthanide-Capped Molecular Capsule, *Inorg. Chem.*, 2007, **46**, 10168-10173.

21 O. A. Gerasko, E. A. Mainicheva, M. I. Naumova, O. P. Yurjeva, A. Alberola, C. Vicent, R. Llusar and V. P. Fedin, Tetranuclear Lanthanide Aqua Hydroxo Complexes with Macrocyclic Ligand Cucurbit[6]uril, *Eur. J. Inorg. Chem.*, 2008, **3**, 416-424.

22 P. Thuéry, Uranyl Ion Complexes with Cucurbit[5]uril: from Molecular Capsules to Uranyl-Organic Frameworks, *Crystal Growth & Design*, 2009, **9**, 1208-1215.

23 W. J. Chen, D. H. Yu, X. Xiao, Y. Q. Zhang, Q. J. Zhu, S. F. Xue, Z. Tao and G. Wei, Difference of coordination between alkali- and alkaline-earth-metal ions to a symmetrical α,α',β,β'-tetramethylcucurbit[6]uril, *Inorg. Chem.*, 2011, **50**, 6956-6964.

24 X. Feng, X. J. Lu, S. F. Xue, Y. Q. Zhang, Z. Tao and Q. J. Zhu, A novel two-dimensional network formed by complexation of cucurbituril with cadmium ions, *Inorg. Chem. Commun.*, 2009, **12**, 849-852.

25 P. Thuéry, Uranyl ion complexes of cucurbit[7]uril with zero-, one- and two-

dimensionality. *CrystEngComm*, 2009, **11**, 1150-1156.

View Article Online
DOI: 10.1039/D0CE01456G

26 X. Xiao, Z. Tao, S. F. Xue, Y. Q. Zhang, Q. J. Zhu, J. X. Liu and G. Wei, Coordination polymers constructed from alkali metal ions and $(HO)_{10}$cucurbit[5]uril, *CrystEngComm*, 2011, **13**, 3794-3800.

27 Z. F. Li, L. L. Liang, F. Wu, F. G. Zhou, X. L. Ni, X. Feng, X. Xiao, Y. Q. Zhang, S. F. Xue, Q. J. Zhu, J. K. Clegg, Z. Tao, L. F. Lindoy and G. Wei, An approach to networks based on coordination of alkyl-substituted cucurbit[5]urils and potassium ions, *CrystEngComm*, 2013, **15**, 1994-2001.

28 N. N. Ji, X. J. Cheng, L. L. Liang, X. Xiao, Y. Q. Zhang, S. F. Xue, Z. Tao and Q. J. Zhu, The synthesis of networks based on the coordination of cucurbit[8]urils and alkali or alkaline earth ions in the presence of the polychloride transition-metal anions, *CrystEngComm*, 2013, **15**, 7709-7717.

29 H. Zhang, R. Zou and Y. Zhao, Macrocycle-based metal-organic frameworks, *Coord. Chem. Rev.*, 2015, **292**, 74-90.

30 P. Thuéry, Structural variations in terbium(III) complexes with 1,3-adamantanedicarboxylate and diverse co-ligands, *J. Solid State Chem.*, 2015, **227**, 265-272.

31 J. Lu, J. X. Lin, X. L. Zhao and R. Cao, Photochromic hybrid materials of cucurbituril and polyoxometalates as photocatalysts under visible light, *Chem. Commun.*, 2012, **48**, 669-671.

32 X. J. Cheng, N. N. Ji, Y. Zhao, L. L. Liang, X. Xiao, Y. Q. Zhang, S. F. Xue, Q. J. Zhu and Z. Tao, $[CdCl_4]^{2-}$ anion-induced coordination of Ln^{3+} to cucurbit[8]uril and the formation of supramolecular self-assemblies: potential application in isolation of light lanthanides, *CrystEngComm*, 2014, **16**, 144-147.

33 P. Thuéry, Second-sphere tethering of rare-earth ions to cucurbit[6]uril by iminodiacetic

acid involving carboxylic group encapsulation, *Inorg. Chem.*, 2010, **49**, 9078-9085.

34 Y. Zhang, S. Panjikar, K. Chen, I. Karatchevtseva, Z. Tao and G. Wei, Lanthanoid Heteroleptic Complexes with Cucurbit[5]uril and Dicarboxylate Ligands: From Discrete Structures to One-Dimensional and Two-Dimensional Polymers, *Inorg. Chem.*, 2019, **58**, 506-515.

35 P. Thuéry, Uranyl Ion Complexation by Aliphatic Dicarboxylic Acids in the Presence of Cucurbiturils as Additional Ligands or Structure-Directing Agents, *Cryst. Growth Des.*, 2011, **11**, 2606-2620.

36 E. A. Kovalenko, D. Y. Naumov and V. P. Fedin, Coordination networks and supramolecular assemblies based on barium cation complexes with cucurbit[6]uril, *Polyhedron*, 2018, **144**, 158-165.

37 A. V. Desai, B. Joarder, A. Roy, P. Samanta, R. Babarao and S. K. Ghosh, Multifunctional Behavior of Sulfonate-Based Hydrolytically Stable Microporous Metal-Organic Frameworks, *ACS Appl. Mater. Interfaces*, 2018, **10**, 39049-39055.

38 M. Cognet, T. Gutel, R. Gautier, X. F. Le Goff, A. Mesbah, N. Dacheux, M. Carboni and D. Meyer, Pillared sulfonate-based metal-organic framework as negative electrode for Li-ion batteries, *Mater. Lett.*, 2019, **236**, 73-76.

39 I. Papadaki, C. D. Malliakas, T. Bakas and P. N. Trikalitis, Molecular supertetrahedron decorated with exposed sulfonate groups built from mixed-valence tetranuclear $Fe_3^{3+}Fe^{2+}(\mu_3\text{-}O)(\mu 3\text{-}SO_4)_3(\text{-}CO_2)_3$ clusters, *Inorg. Chem.*, 2009, **48**, 9968-9970.

40 P. Thuéry and J. Harrowfield, Complexation of Uranyl Ion with Sulfonates: One- to Three-Dimensional Assemblies with 1,5- and 2,7-Naphthalenedisulfonates, *Eur. J. Inorg. Chem.*, 2017, **5**, 979-987.

41 D. K. Panda, K. Maity, A. Palukoshka, F. Ibrahim and S. Saha, Li^+ Ion-Conducting Sulfonate-Based Neutral Metal-Organic Framework, *ACS Sustainable Chem. Eng.*, 2019, **7**,

View Article Online
DOI: 10.1039/D0CE01456G

4619-4624.

42 G. Zhang, G. Wei, Z. Liu, S. R. J. Oliver and H. Fei, A Robust Sulfonate-Based Metal-Organic Framework with Permanent Porosity for Efficient CO_2 Capture and Conversion, *Chem. Mater.*, 2016, **28**, 6276-6281.

43 T. Kurc, J. Janczak, J. Hoffmann and V. Videnova-Adrabinska, New Heterometallic Hybrid Polymers Constructed with Aromatic Sulfonate-Carboxylate Ligands: Synthesis, Layered Structures, and Properties, *Cryst. Growth Des.*, 2012, **12**, 2613-2624.

44 P. Thuéry, Coordination Polymers and Frameworks in Uranyl Ion Complexes with Sulfonates and Cucurbit[6]uril, *Cryst. Growth Des.*, 2011, **11**, 5702-5711.

45 L. Liu, Y. H. Yao, X. F. Zhang, and C. Hao, A Fluorescent 1,5-Naphthalenedisulfonate Anion-Linked Cucurbit[6]uril Framework, *Eur. J. Org. Chem*., 2015, 6806–6810.

46 A. Day, A. P. Arnold, R. J. Blanch and B. Snushall, Controlling Factors in the Synthesis of Cucurbituril and Its Homologues, *J. Org. Chem.*, 2001, **66,** 8094-8100.

47 SAINT, *Program for Data Extraction and Reduction*, Bruker AXS, Inc, Madison, WI, 2001.

48 G. M. Sheldrick, *SADABS*, *Program for Empirical Adsorption Correction of Area Detector Data*, University of Göttingen, Germany, 2003.

49 G. M. Sheldrick, *SHELXT-2014*, *Program for the crystal Structure Solution,* University of Göttingen, Germany, 2014.

50 G. M. Sheldrick, *SHELXL-2018, Program for the crystal Structure refinement,* University of Göttingen, Germany, 2018.

51 A. L. Spek, PLATON, A Multipurpose Crystallographic Tool, Utrecht University, Utrecht, The Netherlands, 2008.

52 Z. Q. Zhu, H. Zhang, Y. W. Li, R. L. Lin, W. Q. Sun, X. F. Chu, J. X. Liu and K. Chen, Anion Influence on Metallosupramolecular Architectures of Cucurbit[6]uril with Calcium

Cation, *Inorg. Chim. Acta*, 2019, **495**, 118900.

View Article Online
DOI: 10.1039/D0CE01456G

53 Z. Y. Hua, C. Chen, F. H. Zhou, H. Zhang, Z. Q. Zhu, W. W. Ge and K. Chen, Anion control in the complexation of cucurbit[6]uril with Cu(II) salts, *Inorg. Chim. Acta*, 2020, **499**, 119183.

54 G. J. Zhao, K. L. Han, Acc. Chem. Res. 2012, 45, 404–413.

55 L. H. Cao, F. Shi, W. M. Zhang, S. Q. Zang and C. W. M. Thomas, Selective sensing of Fe^{3+} and Al^{3+} ions and detection of 2,4,6-trinitrophenol by a water-stable terbium-based metal-organic framework, *Chem. Eur. J.*, 2015, **21**, 15705-15712.

56 X. Y. Dong, R. Wang, J. Z. Wang, S. Q. Zang and T. C. W. Mak, Highly selective Fe^{3+} sensing and proton conduction in a water-stable suflonate-carboxylate Tb-organic-framework, *J. Mater. Chem. A*., 2015, **3**, 641-647.

57 W. N. Yang, J. Li, Z. P. Xu, J. Yang, Y. Liu and L. H. Liu, A Eu-MOF/EDTA-NiAl-ClDH fluorescent micromotor for sensing and removal of Fe^{3+} from water, *J. Mater. Chem. C*., 2019, **7**, 10297-10308.

58 B. Wang, Q. Yang, C. Guo, Y. X. Sun, L. H. Xie and J. R. Li, Stable Zr(Ⅳ)-based metal-organic frameworks with predesigned functionalized ligands for highly selective detection of Fe(Ⅲ) ions in water, *ACS Appl. Mater. Interfaces*, 2017, **9**, 10286-10295.

59 H. H. Li, Y. B. Han, Z. C. Shao, N. Li, C. Huang and H. W. Hou, Water-stable Eu-MOF fluorescent sensor for trivalent metal ions and nitrobenzene, *Dalton Trans.*, 2017, **46**, 12201-12208.

60 H. J. Chen, P. Fan, X. X. Tu, H. Min, X. Y. Yu, X. `eng, S. W. Zhang and P. Cheng, A bifunctional luminescent metal-organic framework for the sensing of paraquant and Fe^{3+} in water, *Chem. Asian. J.*, 2019, **14**, 3611-3619.

61 M. Chen, W. M. Xu, J. Y. Tian, H. Cui, J. X. Zhang, C. S. Liu and M. Du, A terbium(III) lanthanide-organic framework as a platform for a recyclable multi-responsive luminescent

sensor, *J. Mater. Chem. C.,* 2017, **5**, 2015-2021.

View Article Online
DOI: 10.1039/D0CE01456G

62 J. C. Jin, L. Y. Pang, G. P. Yang, L. Hou and Y. Y. Wang, Two porous luminescent metal-organic frameworks: quantifiable evaluation of dynamic and static luminescent sensing mechanisms towards Fe^{3+}, *Dalton Trans.*, 2015, **44**, 17222-17228.

63 D. Zhao, X. H. Liu, Y. Zhao, P. Wang, Y. Liu, M. Azam, S. I. AI-Resayes, Y. Lu and W. Y. Sun, Luminescent Cd(Ⅱ)-organic frameworks with chelating NH_2 sites for selective detection of Fe^{3+} and antibiotics, *J. Mater. Chem. A*., 2017, **5**, 15797-15807.

64 H. Xu, J. Gao, X. Qian, J. Wang, H. He, Y. Cui, Y. Yang, Z. Wang and G. D. Qian, Metal-organic framework nanosheets for fast-response and highly sensitive luminescent sensing of Fe^{3+}, *J. Mater. Che m. A.*, 2016, **4**, 10900-10905.

65 X. Y. Dong, R. Wang, J. Z. Wang, S. Q. Zang, T. C. W. Mak, Highly selective Fe^{3+} sensing and proton conduction in a water-stable sulfonate-caboxylate Tb-organic-framework, *J. Mater. Chem. A.*, 2015, **3**, 641-647.

66 G. Liu, Y.-K. Lu, Y.-Y. Ma, X.-Q. Wang, L. Hou and Y.-Y. Wang, Syntheses of three new isostructural lanthanide coordination polymers with tunable emission colours through bimetallic doping, and their luminescence sensing properties, Dalton Trans., 2019, 48, 13607-13613.

67 G.-P. Li, G. Liu, Y.-Z. Li, L. Hou, Y.-Y. Wang, and Z. H. Zhu, Uncommon Pyrazoyl-Carboxyl Bifunctional Ligand-Based Microporous Lanthanide Systems: Sorption and Luminescent Sensing Properties, Inorg. Chem. 2016, 55, 8, 3952–3959.

For Table of Contents Use Only:

View Article Online
DOI: 10.1039/D0CE01456G

Assemblies of Cucurbit[6]uril-Based Coordination Complexes with Disulfonate Ligands: From Discrete Complexes to One- and Two-Dimensional Polymers

Kai Chen*, †, Zi-Yi Hua,† Ran Li, † Yu-Ying Peng,† Qiang Zhao Zhu, † Carl Redshaw ‡

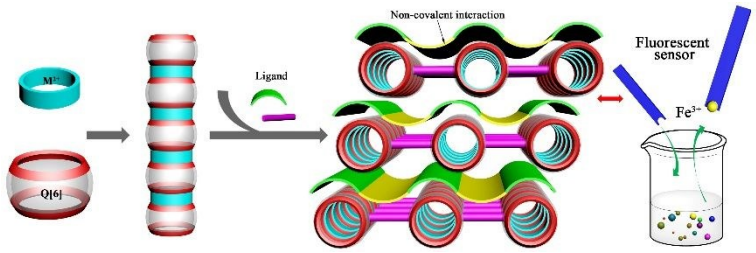

Nine assemblies of Q[6]-based coordination complexes incorporating disulfonate ligands were obtained and two of them found to have ability for sensing Fe^{3+} *via* fluorescence quenching effect.

View Article Online
DOI: 10.1039/D0CE01456G

Table 1. Crystal Data and Structure Refinements for **1-9** [a].

Compound	**1**	**2**	**3**	**4**	**5**
chemical formula	$C_{28}H_{38}N_{12}O_{19}S_2$ Ca	$C_{28}H_{40}N_{12}O_{20}S_2$ Sr	$C_{28}H_{40}N_{12}O_{20}S$ $_2$Ba	$C_{28}H_{52}N_{12}O_{26}S_2$ Ca	$C_{28}H_{50}N_{12}O_{25}$ S_2Sr
formula weight	950.87	1016.43	1066.12	1076.98	1076.98
crystal system	Triclinic	Triclinic	Triclinic	Monoclinic	Monoclinic
space group	*P*-1	*P*-1	*P*-1	$P2_1/n$	$P2_1/n$
a /Å	10.540(5)	10.770(5)	11.2440(6)	16.5541(13)	16.623(4)
b /Å	14.070(5)	14.128(5)	13.9869(8)	10.4598(8)	10.715(2)
c /Å	15.113(5)	15.073(5)	14.8283(8)	25.6563(19)	25.723(6)
α /°	110.556(5)	110.391(5)	109.442(2)	90	90
β /°	106.367(5)	107.230(5)	111.672(2)	90.830(3)	90.124(4)
γ /°	102.044(5)	101.991(5)	99.695(2)	90	90
temperature /K	293(2)	293(2)	173(2)	173(2)	296(2)
volume /Å^3	1891.8(13)	1925.5(13)	1927.38(19)	4442.0(6)	4581.7(18)
Z	2	2	2	4	4
D_c /g cm^{-3}	1.588	1.643	1.727	1.353	1.381
μ /mm^{-1}	0.368	1.598	6.704	1.845	1.344
F(000)	928	964	1000	1856	1928
reflections collected/unique	10360 / 6599	10886 / 6762	21316 / 6794	52610 / 7867	33674 / 8059
data / restraints / parameters	6599 / 12 / 541	6762 / 0 / 541	6794 / 0 / 536	7867 / 19 / 541	8059 / 78 / 570
GOF	1.011	1.021	1.036	1.033	1.048
R_1, wR_2 [$I > 2\sigma(I)$][a,b]	R_1 = 0.0563, wR_2 = 0.1517	R_1 = 0.0464, wR_2 = 0.1140	R_1 = 0.0698, wR_2 = 0.1878	R_1 = 0.0667, wR_2 = 0.1923	R_1 = 0.0649, wR_2 = 0.1783
R_1, wR_2 (all data)	R_1 = 0.1140, wR_2 = 0.1726	R_1 = 0.0743, wR_2 = 0.1228	R_1 = 0.0763, wR_2 = 0.1953	R_1 = 0.0745, wR_2 = 0.1996	R_1 = 0.0968, wR_2 = 0.1955

View Article Online
DOI: 10.1039/D0CE01456G

Compound	**6**	**7**	**8**	**9**
chemical formula	$C_{56}H_{84}N_{24}O_{41}S_4Ba_2$	$C_{28}H_{46}N_{12}O_{23}S_2Sr$	$C_{56}H_{85}N_{24}O_{48}S_4Ca_2$	$C_{46}H_{66}N_{24}O_{30}S_2Sr$
formula weight	2152.31	1070.48	2070.82	1586.91
crystal system	Monoclinic	Triclinic	Orthorhombic	Monoclinic
space group	*C*2/c	*P*-1	$P2_12_12$	$P2_1/n$
a /Å	27.899(3)	10.714(5)	25.565(3)	12.604(5)
b /Å	15.2073(16)	14.407(5)	31.743(3)	16.258(5)
c /Å	39.875(5)	15.630(5)	10.3985(11)	31.463(5)
α /°	90	65.529(5)	90	90
β /°	106.296(2)	73.674(5)	90	97.344(5)
γ /°	90	86.240(5)	90	90
temperature /K	293(2)	293(2)	293(2)	293(2)
volume /Å^3	16238(3)	2103.8(14)	8438.4(15)	6394(3)
Z	8	2	4	4
D_c /g cm^{-3}	1.587	1.503	1.424	1.507
μ /mm^{-1}	1.160	1.463	0.330	1.003
F(000)	7744	964	3708	2960
reflections collected / unique	43541 / 14290	11786 / 7352	62113 / 14860	35466 / 11252
data / restraints / parameters	14290 / 24 / 1075	7352 / 0 / 541	14860 / 32 / 1082	11252 / 0 / 865
GOF	1.015	1.024	1.068	1.032
R_1, wR_2 [$I > 2\sigma(I)$][a,b]	$R_1 = 0.0476$, $wR_2 = 0.1157$	$R_1 = 0.0437$, $wR_2 = 0.1189$	$R_1 = 0.0600$, $wR_2 = 0.1598$	$R_1 = 0.0592$, $wR_2 = 0.1593$
R_1, wR_2 (all data)	$R_1 = 0.0616$, $wR_2 = 0.1227$	$R_1 = 0.0559$, $wR_2 = 0.1247$	$R_1 = 0.0639$, $wR_2 = 0.1629$	$R_1 = 0.0908$, $wR_2 = 0.1729$

[a] $R_1 = \Sigma||F_o| - |F_c||/\Sigma|F_o|$. [b] $wR_2 = |\Sigma w(|F_o|^2 - |F_c|^2)|/\Sigma|w(F_o)^2|^{1/2}$, where $w = 1/[\sigma^2(F_o^2) + (aP)^2 + bP]$. $P = (F_o^2 + 2F_c^2)/3$